

Distributed fixed resources exchanging particles: Phases of an asymmetric exclusion process connected to two reservoirs

Sourav Pal,^{1,*} Parna Roy,^{2,†} and Abhik Basu^{1,‡}

¹*Theory Division, Saha Institute of Nuclear Physics, A CI of Homi Bhabha National Institute, 1/AF Bidhannagar, Calcutta 700064, West Bengal, India*

²*Shahid Matangini Hazra Government General Degree College for Women, Purba Medinipore 721649, West Bengal, India*

We propose and study a conceptual one-dimensional model to explore how the combined interplay between fixed resources and particle exchanges between different parts of an extended system can affect the stationary densities in a current carrying channel connecting different parts of the system. To this end, we consider a model composed of a totally asymmetric simple exclusion process (TASEP) connecting two particle reservoirs without any internal dynamics but which can directly exchange particles between each other, ensuring nonvanishing currents in the steady states. The total particle number in the system that defines the “resources” available, although is kept constant by the model dynamics, can take any value independent of the model parameters that define the dynamics of the model. We show how the resulting phase diagrams of the model are controlled by the parameters, which define the various dynamical update rules together with the total available resources. These control parameters can be tuned to make the density on the TASEP lane globally uniform or piecewise continuous with localized domain walls, and can also control populations of the two reservoirs. In general, the phase diagrams are quite different from a TASEP with open boundaries. In the limit of large amount of resources, the phase diagrams in the plane of the control parameters become topologically identical to that for an open TASEP together with delocalization of domain walls.

I. INTRODUCTION

Far-from-equilibrium phenomena are ubiquitous in nature, which, in contrast to their equilibrium counterparts, are yet to be fully explored. Studies on driven diffusive systems are fundamentally important to understand the rich behaviour of low dimensional collective particle transport in nonequilibrium systems. A particularly important model is the Totally Asymmetric Simple Exclusion Process (TASEP), originally proposed to study protein synthesis in biological cells [1]. Subsequently, it has been used as a paradigmatic one-dimensional (1D) open model that shows boundary-induced phase transitions [2–4]. A TASEP consists of a 1D lattice with L sites having open boundaries. The dynamics is stochastic in nature, and involves unidirectional particle hopping, subject to exclusion at all the sites, i.e., any site can contain at most one particle at a time. In a TASEP, a particle enters at the left boundary ($i = 1$) of the 1D lattice at a given rate α_T , hops unidirectionally to the following sites at rate unity subject to exclusion until it reaches the last site at the other end ($i = L$), from which it leaves the system at another specified rate β_T . Controlled by α_T and β_T , the TASEP exhibits three distinct phases: the steady state densities in bulk can be either less than half, which is the low-density (LD) phase, or more than half, forming the high-density (HD) phase, or just half, which is the maximal current (MC) phase of

TASEP. Furthermore, in the $\alpha_T - \beta_T$ plane there is a co-existence line separating the LD and HD phases, where nonuniform densities in the form of a domain wall (DW) can be found. This DW is *delocalized*, a property that is attributed to the particle nonconserving dynamics governing the open TASEP [5].

A periodic TASEP on a uniform ring necessarily has a constant mean density, owing to the translational invariance of the system. Macroscopically nonuniform densities can be expected only when the translational invariance is broken. This can be achieved by, for instance, the presence of bottlenecks, point [6, 7] or extended (either a slower segment or a segment executing diffusive motion) [8–12], or a combination of both [13]. A TASEP with open boundaries does not have any particle number conservation, whereas a TASEP on a ring obviously conserves the total particle number. A third possibility is an open TASEP with a global constraint on the total particle number, or equivalently, a closed system of a TASEP connected to a particle reservoir of finite capacity or a particle storage; see, e.g., Refs. [14, 15]. More than one TASEP connected to a reservoir has also been considered; see Ref. [16]. A closed system containing a TASEP and a reservoir manifestly breaks the translation invariance, and hence is a potential candidate for inhomogeneous steady state densities. These are also expected to be relevant in related biological processes of protein synthesis in cells [14] and also in the context of traffic [17]; see also Ref. [18] for a similar study. Detailed studies, both numerical MCS and analytical MFT reveal rich nonuniform steady state density profiles including domain walls in these models [14–16]. The ideas behind a TASEP connected to a particle storage of finite capacity have been applied to various different problems,

*Electronic address: isourav81@gmail.com

†Electronic address: parna.roy14@gmail.com

‡Electronic address: abhik.123@gmail.com, abhik.basu@saha.ac.in

e.g., limited resources in driven diffusive systems [19], different biological contexts like mRNA translations and motor protein dynamics in cells [20, 21] and traffic problems [17]. Notable experimental studies relevant to these model systems include studies on spindles in eukaryotic cells [22, 23].

A fundamentally important question in nonequilibrium systems is the consequence of coupling driven with equilibrium processes on the steady states. In particular, we are interested in how asymmetric exclusion process, a paradigmatic nonequilibrium process, couples with equilibrium diffusive exchanges to produce nontrivial steady states. Diffusion is quite common in cell biology [24]. Molecular motors in cells undergo driven motion along the microtubules, which are quasi-1D channels, or diffusion in the cell cytoplasm embedding the microtubules, providing a natural example to study the mutual interplay between driven and equilibrium dynamics. Such interplay between driven and diffusive dynamics has been explored by studying a variety of models. These are characterised by specific descriptions of particle diffusion, how it couples to the driven part (e.g., TASEP) of the dynamics and the role of any global conservation laws. For instance, the consequences of the effects of diffusion on the steady states of the filament (TASEP) has been explored in Refs. [25–29], by generally modeling the system as a filament (microtubule) executing TASEP confined in a three-dimensional (3D) particle reservoir representing the cell cytoplasm, where the motors diffuse around. In an approach that is complementary to these 3D model studies, a two-lane system has been considered with one lane being a TASEP and the other executing simple exclusion process (SEP), a 1D representation of diffusion. This has been considered in closed [9, 11], half-open [30, 31] and open geometries [32], each revealing the nontrivial steady states borne by the interplay between TASEP and SEP.

Although significant progress has been made in the research in TASEPs with finite resources, there are still unresolved questions. In a recent study on a similar model consisting of a single TASEP lane connected to two reservoirs at both its ends [33], it has been shown that in general for a given total particle number, a conserved quantity, not all the phases of an open TASEP may be realised by the TASEP in that model. Further, it has been argued in Ref. [33] that when the particle exchanges between the two reservoirs compete with the particle hopping in the TASEP, the effects of fluctuations remain significant *even* in the thermodynamic limit, in contrast to when the particle exchange processes dominate over the TASEP current. As a result, the phase diagrams in the two cases can be quite different from each other. Furthermore, not only there is a strict global conservation law, there is also a strict upper limit on the number of particles that can be accommodated, given a set of the model parameters that define the dynamical updates, in the model of Ref. [33], for which the model is completely filled with the TASEP bulk density reach-

ing unity. A consequence of this is that this model *never* reduces to an ordinary TASEP, even for a very large admissible number of total particles (possible for specific choices of the model parameters). Since the model in Ref. [33] is effectively a *two-constraint* model, a pertinent question is what happens when one of them is lifted. To that end, we construct and study a conceptual model whose dynamics necessarily *conserves the total particle number*, but has *no upper limit* on the admissible total particle number for any value of the dynamical model parameters.

In this work, we focus on a TASEP connected to two particle reservoirs, which can also directly exchange particles between them. The latter process ensures a finite steady state current through the TASEP. The actual entry to and exit rates from the TASEP, being dependent on the “supply side” and “receiving side” instantaneous reservoir populations through some functions of these populations parametrised by two constants α and β , are dynamically derived quantities; see next Section for details. Our model is constructed in such a way that it (i) strictly conserves the total particle number (covering the TASEP lane and the two reservoirs), but (ii) can accommodate any number of particles (including a diverging number of particles approaching infinity) for *any values* of the model parameters which define the dynamical update rules. This stands in stark contrast to a similar model with a single TASEP channel connected to two reservoirs exchanging particles [33], where unlimited accommodation of particles is generally not possible. This has a strong consequence: in the present study, the phase diagram of our model smoothly reduces to one that is topologically identical to that for an open TASEP in the limit of large (formally diverging) number of total particles for *any* choices of the model parameters that define the update rules. This does not hold true for the model in Ref. [33]. Lastly, with increasing total available particle number or “resources”, a localized DW in this model gradually delocalizes. We study our model in two different limits: (i) when the particle exchanges between the reservoirs compete with the hopping along the TASEP, called weak coupling limit, and (ii) when the former overwhelms the latter, designated as the strong coupling limit of the model.

The remaining parts of this article are organised as follows. In Section II, we define our model and give the dynamical update rules. It is then followed by setting up a mean-field analysis of the steady state densities in the weak coupling limit given in Section III. Next, in Section IV phase diagrams are obtained using analytical mean-field theory corroborated by Monte Carlo simulation. The steady state densities and phase boundaries are derived in Section V; wherein in Section VF the nature of the phase transitions of the model is discussed. We summarise the findings in Section VIII. Our results on the strong coupling limit are given in the Appendix.

II. THE MODEL

Our model consists of a 1D lattice T having L sites, connected to two particle reservoirs R_1 and R_2 at both ends. The reservoirs are considered to be point reservoirs without any internal structure or dynamics. The hard-core exclusion principle enforces that each site of T can hold a maximum of one particle at any given moment. The lattice T executes TASEP dynamics [33]. Provided the first site of T is empty, a particle from R_1 enters T with a rate α_{eff} that depends on the instantaneous population of R_1 . The particle then hops clockwise to the next available site. The hopping rate in the bulk of T is taken to be unity to set the time scale. Eventually, after reaching the last site of T , the particle jumps into R_2 with a rate β_{eff} that depends on the instantaneous population of R_2 . The closed geometry of the model ensures the overall particle number (including both the TASEP lane and reservoirs), N_0 , to be conserved. This can be expressed as

$$N_0 = N_1 + N_2 + \sum_{i=1}^L n_i, \quad (1)$$

where N_1, N_2 are the number of particles in R_1, R_2 respectively, and n_i 's are binary variables denoting the occupation number of sites $i = 1, 2, \dots, L$ in the TASEP lane. We choose $n_i = 0$ for vacant sites and $n_i = 1$ for occupied ones. The dynamical dependence of effective rates α_{eff} and β_{eff} on the instantaneous populations N_1 and N_2 of the reservoirs R_1 and R_2 can be expressed as following:

$$\alpha_{\text{eff}} = \alpha f(N_1); \quad \beta_{\text{eff}} = \beta g(N_2), \quad (2)$$

where f and g are functions of N_1 and N_2 respectively. Inflow of particles from R_1 to T increases with the rising population of R_1 , whereas the outflow of particles from T to R_2 should be hindered by the growing population in R_2 . This suggests that f and g should be monotonically increasing and decreasing functions of N_1 and N_2 respectively. We choose the following simple functions which captures these criteria:

$$f(N_1) = \frac{N_1}{N_0}, \quad g(N_2) = 1 - \frac{N_2}{N_0}. \quad (3)$$

Similar functions have been used elsewhere before; see, e.g., Refs. [34–37]. Notice that the choices (3) are *different* from those used in Refs. [14–16, 33]. The rate functions in the latter studies have the TASEP size L appearing as a normalisation constant, whereas in the present study as well as those in Refs. [34–37], N_0 appears as the normalisation constant. While this may appear as a minor technical matter, our results show that depending upon these choices, the results can change significantly.

In our model, the upper limit on each of N_1, N_2 can be N_0 , the total particle number, or the “total available resources” in the system. Further, we do not restrict N_0

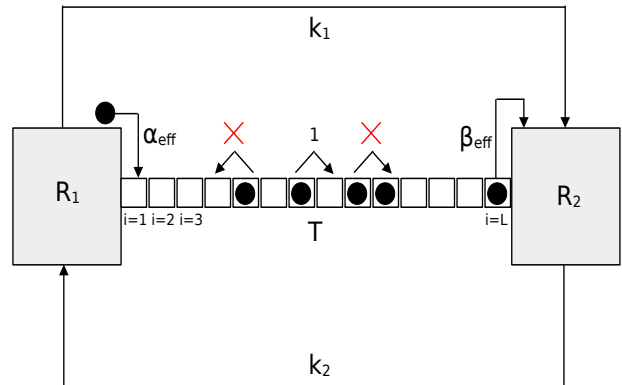


FIG. 1: **Schematic diagram of the model:** Here, R_1 and R_2 are two particle reservoirs, both connected to a TASEP lane T with L sites at its both ends. Particles, represented by black solid circles, enter the first site ($i = 1$) of T from R_1 with a rate α_{eff} , followed by hopping to the sites on the right side with a rate of unity, subject to exclusion. Eventually, particles exit from the last site ($i = L$) of T to go to R_2 with a rate of β_{eff} . Furthermore, particle exchanges occur directly between R_1 and R_2 with rates k_1 and k_2 , modelling diffusion in the system (see text).

to be finite, i.e., N_0 can take *any* value including approaching infinity. Thus N_1 and N_2 can also grow indefinitely, independent of the other model parameters. This is in stark contrast to the model studied in Ref. [33]. The rate functions f and g have the following properties: (i) $f(0) = 0$, (ii) $f(\infty) = 1$, (iii) $g(0) = 1$, and (iv) $g(\infty) = 0$. In general, the rate functions f and g have values between 0 and 1. In addition to particle hopping motion in T , the reservoirs can directly exchange particles between them with certain rates to maintain a nonzero current in T : R_1 (R_2) releases particles at rate k_1 (k_2) which R_2 (R_1) receives instantaneously. We define a parameter $\mu = N_0/L$ to denote the availability of particles in the system. Since the total particle number, N_0 , has no upper limit, μ can be any positive real number: $0 \leq \mu < \infty$. Taken together, our model has five control parameters: α, β, μ, k_1 , and k_2 , same as the model studied in Ref. [33].

III. MEAN-FIELD THEORY

We now set up the mean-field theory (MFT) for our model by following the same line of reasoning as in previous studies [38]. MFT involves neglecting the correlation effects and replacing averages of products by the prod-

ucts of averages. The ensuing MFT equations take the same form as those in Ref. [33], which we revisit here for the convenience of the readers. Considering the density ρ_i as the time-average of occupation number n_i at site i , $\rho_i \equiv \langle n_i \rangle$, we have the following equations of motion for the bulk sites $1 < i < L$ in MFT:

$$\frac{d\rho_i}{dt} = \rho_{i-1}(1 - \rho_i) - \rho_i(1 - \rho_{i+1}). \quad (4)$$

For the boundary sites ($i = 1$ and $i = L$), we have

$$\frac{d\rho_1}{dt} = \alpha_{\text{eff}}(1 - \rho_1) - \rho_1(1 - \rho_2), \quad (5)$$

$$\frac{d\rho_L}{dt} = \rho_{L-1}(1 - \rho_L) - \beta_{\text{eff}}\rho_L. \quad (6)$$

Similarly, the time-evolution of reservoir populations N_1 and N_2 are represented by the following equations:

$$\frac{dN_1}{dt} = k_2N_2 - k_1N_1 - J_{T-in}, \quad (7)$$

$$\frac{dN_2}{dt} = k_1N_1 - k_2N_2 + J_{T-out}, \quad (8)$$

where $J_{T-in} = \alpha_{\text{eff}}(1 - \rho_1)$ and $J_{T-out} = \beta_{\text{eff}}\rho_L$ are, respectively, the incoming and outgoing currents in the TASEP.

Now, introduce a quasi-continuous variable $x = i/L \in [0, 1]$ where $\epsilon = 1/L$ is the lattice constant [33]. The density at a position x at time t is denoted by $\rho(x, t) \equiv \rho_i(t)$. As shown in Ref. [33], the discrete equation of motion [Eq. (4)] takes a conservation law form

$$\frac{\partial \rho(x, t)}{\partial t} = -\epsilon \partial_x (\rho(x)[1 - \rho(x)]) + \mathcal{O}(\epsilon^2), \quad (9)$$

supplemented by the boundary conditions $\rho(0) = \alpha_{\text{eff}}$, $\rho(1) = 1 - \beta_{\text{eff}}$. Eq. (9) has a conservation law form, reflecting the conserving nature of the TASEP dynamics in the bulk, and thus allows us to extract a mean-field particle current J_T in the bulk

$$J_T = \rho(1 - \rho), \quad (10)$$

which becomes a constant in the steady state, along with $J_{T-in} = J_{T-out} = J_T$ in the steady states.

In the nonequilibrium steady states, the reservoir populations are constants over time in MFT. Hence,

$$\frac{dN_1}{dt} = \frac{dN_2}{dt} = 0. \quad (11)$$

Substituting Eq. (11) in Eqs. (7) and (8), we get

$$k_2N_2 = k_1N_1 + J_T. \quad (12)$$

Eq. (12) is a flux balance equation relating the particle current J_T with the reservoir populations N_1 and N_2 .

As discussed in Ref. [33], the solution of Eq. (10) gives the steady state densities

$$\rho = \frac{1}{2} \left(1 \pm \sqrt{1 - 4J_T} \right) := \rho_{\pm}. \quad (13)$$

Thus, ρ can exhibit spatial uniformity with a low-density (LD) phase characterised by $\rho = \rho_- \leq 1/2$ and a high-density (HD) phase characterised by $\rho = \rho_+ > 1/2$. Additionally, a maximum current (MC) phase can arise with $J_T = 1/4$ when $\rho = 1/2$. Another possibility is the presence of a macroscopic nonuniformity in density in the form of a domain wall connecting the LD and HD domains, which is the domain wall (DW) phase or a shock phase.

When solved for N_1 and N_2 , Eq. (12) along with PNC, $N_0 = N_1 + N_2 + N_T$, where $N_T \equiv L \int_0^1 \rho(x) dx$ is the number of particles in the TASEP lane, gives [33]

$$N_1 = \frac{k_2(N_0 - N_T) - J_T}{k_1 + k_2}, \quad (14a)$$

$$N_2 = \frac{k_1(N_0 - N_T) + J_T}{k_1 + k_2}. \quad (14b)$$

Thus, N_1, N_2 depend upon J_T explicitly, and also implicitly through the dependence of N_0 on J_T .

Similar to Ref. [33], we consider two distinct cases. We have $J_T < 1$ ($J_{\text{max}} = 1/4$), whereas N_1 and N_2 rise with L , since N_0, N_T scale with L for a given μ . Thus, if $k_{1,2} \sim \mathcal{O}(1)$, we can neglect J_T safely in Eq. (12) in the thermodynamic limit (TL). Similarly, we note that in Eqs. (14a) and (14b), where $J_T < 1$, but N_0 and N_T should rise with L indefinitely. Thus, if $k_{1,2} \sim \mathcal{O}(1)$, we can neglect J_T in TL, giving $k_1N_1 = k_2N_2$ asymptotically exact, independent of J_T . Therefore, in TL, the relative population of the two reservoirs is controlled by just the ratio k_2/k_1 , and independent of J_T, α , and β . This effectively eliminates one of the reservoirs, enabling us to describe the steady state in terms of an effective single reservoir. This is the diffusion dominated regime, named *strong coupling limit* below. Another regime of interest, where diffusion process competes with hopping, is also discussed. We call this *weak coupling limit*, which can be achieved by introducing a mesoscopic scaling $k_{1(2)} = k_{10(20)}/L$ where $k_{10,20} \sim \mathcal{O}(1)$. In this case, the general solutions for the reservoir populations N_1 and N_2 in the MFT are given by

$$N_1 = \frac{k_{20}(N_0 - N_T) - LJ_T}{k_{10} + k_{20}}, \quad (15a)$$

$$N_2 = \frac{k_{10}(N_0 - N_T) + LJ_T}{k_{10} + k_{20}}, \quad (15b)$$

revealing their explicit J_T -dependence, which do not vanish in the limit $L \rightarrow \infty$, since both N_0, N_T also scale linearly with L for a fixed μ . This ensures competition between J_T and the other contributions in (15a) and (15b). In the main text of the paper, phase diagrams and density profiles in weak coupling limit are discussed elaborately. We discuss the strong coupling limit case in the Appendix. Although these classifications of weak and strong coupling cases of our model are identical to those

in Ref. [33], as in both the models these are done in terms of the scaling of k_2 , k_2 with L , nonetheless, we show below that the results from the present study are significantly different from those obtained in Ref. [33] due to the fundamentally different forms for the rate functions f and g .

IV. MEAN-FIELD PHASE DIAGRAMS IN THE WEAK COUPLING CASE

Before presenting the phase diagrams of the present model, we briefly revisit the usual open TASEP model [38]. The phase diagram of an open boundary TASEP, with $\alpha_T, \beta_T < 1$ as the entry and exit rates which are the control parameters, exhibits three distinct phases: an entry-limited low-density (LD) phase with bulk density $\rho_{LD} < 1/2$, an exit-limited high-density (HD) phase with bulk density $\rho_{HD} > 1/2$, and a bulk-limited maximal current (MC) phase with bulk density $\rho_{MC} = 1/2$. Conditions for the occurrence of these phases are as follows: for the LD phase, we have $\rho_{LD} = \alpha_T < \beta_T$ and $\alpha_T < 1/2$; for the HD phase, we have $1 - \rho_{HD} = \beta_T < \alpha_T$ and $\beta_T < 1/2$, and for the MC phase, we have $\alpha_T, \beta_T \geq 1/2 = \rho_{MC}$. On the coexistence line between (0,0) and (1/2,1/2), which corresponds to points with $\alpha_T = \beta_T < 1/2$, the bulk density in T exhibits a piecewise discontinuity, forming a domain wall (DW) that connects the LD and HD domains together. This domain wall spans the entire lattice instead of being confined to a specific region and hence is delocalized. This is attributed to the particle number nonconservation in the model due to the stochastic entry-exit events. The conditions for transitions between different phases in an open TASEP can be obtained by equating the currents in the respective phases. Specifically, the transition from LD to HD phases occurs when $\alpha_T = \beta_T < 1/2$. Likewise, the transitions from LD to MC and from HD to MC occur when $\alpha_T = 1/2 < \beta_T$ and $\beta_T = 1/2 < \alpha_T$, respectively. In the $\alpha_T - \beta_T$ plane, the three phases intersect at a common point (1/2,1/2). The LD-HD transition manifests as a sudden change in the bulk density, indicating a first-order phase transition. In contrast, the transitions from either LD or HD to the MC phase involve a continuous variation in the bulk density, indicating a second-order phase transition.

Fig. 2 gives the phase diagrams of our model in the $\alpha - \beta$ plane in the weak coupling limit for various μ together with exchange rates $k_{10} = 0$ and $k_{20} = 0.95$, where the different phases are delineated by comparing them with those found in an open TASEP. The structure of these phase diagrams in Fig. 2 is quite sensitive to the values of μ . The steady state bulk density in the LD phase is $\rho_{LD} = \alpha_{\text{eff}}$, while in the HD phase, $\rho_{HD} = 1 - \beta_{\text{eff}}$. In an open TASEP, phase transitions between different phases can be determined by equating the currents corresponding to each phase. Extending that principle to the present case, the transition from the LD to the HD phase

occurs when $\alpha_{\text{eff}} = \beta_{\text{eff}} < 1/2$. Similarly, the transitions between the LD and MC phases, as well as between the HD and MC phases, are characterised by the conditions $\alpha_{\text{eff}} = 1/2 < \beta_{\text{eff}}$ and $\beta_{\text{eff}} = 1/2 < \alpha_{\text{eff}}$, respectively.

The phase diagram with $\mu = 0.5$ [see Fig. 2 (top left)], there are only LD and DW phases. Indeed, with such a low value of μ , there are fewer particles and hence the existence of the HD and MC phases in the TASEP lane is *not* possible. We find that this particular phase pattern persists up to $\mu = 0.76$ for $k_{10} = 0$ and $k_{20} = 0.95$. As μ exceeds this threshold, the MC and HD phases start to emerge. Consequently, the phase diagrams with $\mu > 0.76$ consist of all four phases, namely LD, HD, MC, and DW phase, see the phase diagrams corresponding to $\mu = 1$ and $\mu = 1.5$ in Fig. 2. The phase boundary between the LD(HD) and MC phases appears as a straight line parallel to the β -(α -)axis in both MFT and Monte Carlo simulation (MCS) studies. Noticeable deviations, however, between MFT and MCS outcomes are observed in obtaining these phase boundaries as μ grows. As μ increases further, the HD phase expands while the DW region shrinks accordingly, see the phase diagram with $\mu = 1.5$. Surprisingly, when μ is raised to a significantly large value, such as $\mu = 100$, only three distinct phases, namely LD, HD, and MC, are visible in the phase space. The DW phase region now gets contracted into an inclined line extending from (0,0) to (1/2,1/2). The domain wall spans the whole of the TASEP lane without any specific or unique position, and hence is a delocalized domain wall (DDW).

In the following sections, we calculate the steady state density profiles in the different phases and the boundaries separating them in MFT.

V. STEADY STATE DENSITIES AND PHASE BOUNDARIES

A. Low-density phase

In the LD phase, steady state bulk density is given by

$$\rho_{LD} = \alpha_{\text{eff}} = \alpha \frac{N_1}{N_0} < \frac{1}{2}. \quad (16)$$

Substituting N_1 from Eq. (14a) in Eq. (16) and identifying the steady state particle current in the LD phase as $J_{LD} = \rho_{LD}(1 - \rho_{LD})$, we obtain a quadratic equation in ρ_{LD} :

$$\rho_{LD} = \alpha \left[\frac{k_2}{k_1 + k_2} \left(1 - \frac{\rho_{LD}}{\mu} \right) - \frac{\rho_{LD}(1 - \rho_{LD})}{N_0(k_1 + k_2)} \right]. \quad (17)$$

Now in the weak coupling limit, particle exchange rates $k_{1(2)} = k_{10(20)}/L$. Substituting that in Eq. (17) and recalling $N_0 = \mu L$, we get

$$\rho_{LD} = \alpha \left[\frac{k_{20}}{k_{10} + k_{20}} \left(1 - \frac{\rho_{LD}}{\mu} \right) - \frac{\rho_{LD}(1 - \rho_{LD})}{\mu(k_{10} + k_{20})} \right]. \quad (18)$$

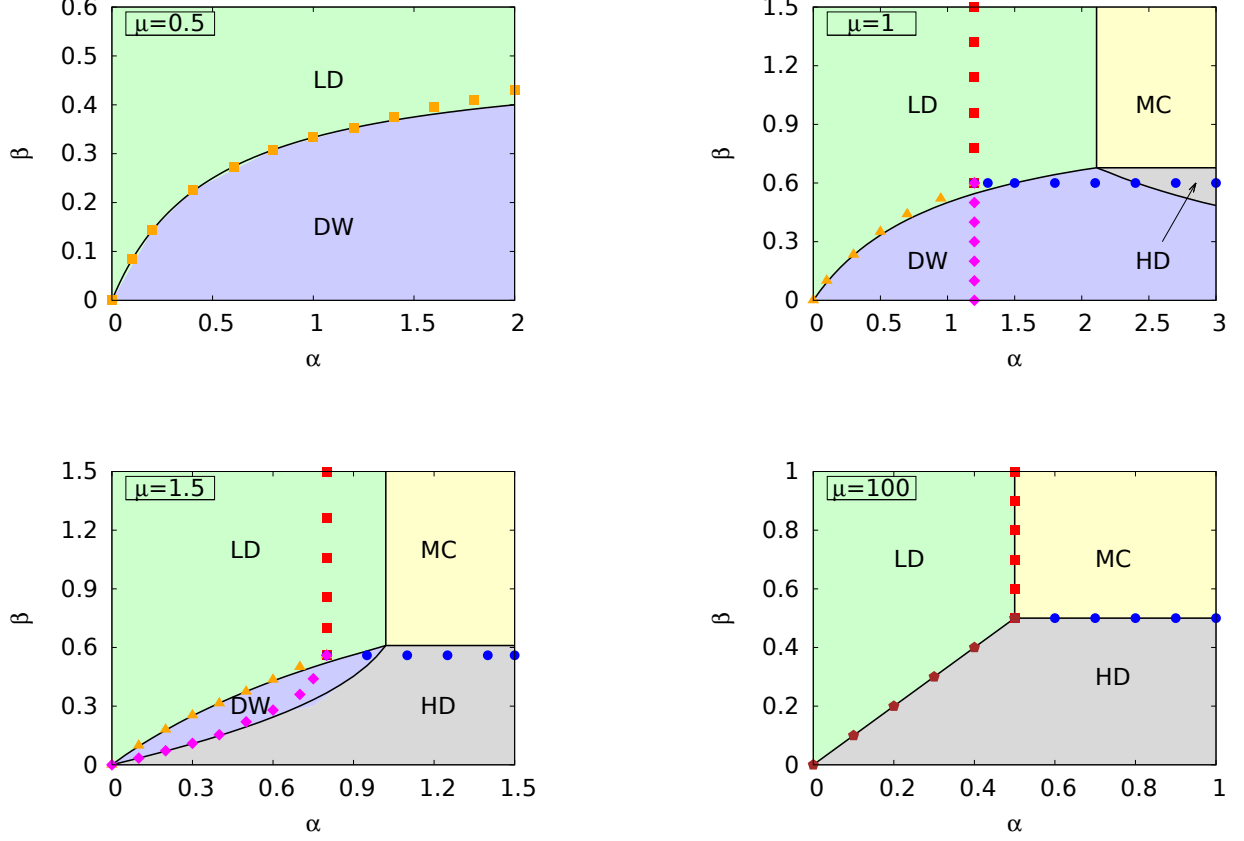


FIG. 2: Phase diagrams in the $\alpha - \beta$ plane with different values of the filling factor μ in the weak coupling limit of the model, with exchange rates $k_{10} = 0$ and $k_{20} = 0.95$. The LD, HD, MC, and DW phases are denoted respectively by green, gray, yellow, and blue regions with solid black lines as the phase boundaries, according to MFT; see Eqs. (34), (35), (56), and (57). The phase boundaries obtained from MCS are represented by discrete colored points: red (LD-MC), blue (HD-MC), orange (LD-DW), and magenta (HD-DW). Noticeable deviations between the theoretical and simulated phase diagrams are observed for intermediate values of μ . Either two or four phases can be simultaneously observed for small or intermediate values of μ . Interestingly, for large values of μ (e.g., $\mu = 100$), the phase diagram of our model exhibits a structure similar to an open TASEP without any noticeable discrepancies between MFT and MCS results, with LD, HD, and MC phases become visible and the DW phase region contracts to an inclined line.

Solving Eq. (18) for ρ_{LD} , we get two solutions:

$$\rho_{LD}^{\pm} = \left(\frac{1 + k_{20}}{2} + \frac{\mu(k_{10} + k_{20})}{2\alpha} \right) \pm \left[\left(\frac{1 + k_{20}}{2} + \frac{\mu(k_{10} + k_{20})}{2\alpha} \right)^2 - \mu k_{20} \right]^{\frac{1}{2}}. \quad (19)$$

The condition that $\rho_{LD} \rightarrow 0$ when $\mu \rightarrow 0$ establishes the following as the physically acceptable solution for the LD phase density:

$$\rho_{LD} = \rho_{LD}^{-} = \left(\frac{1 + k_{20}}{2} + \frac{\mu(k_{10} + k_{20})}{2\alpha} \right) - \left[\left(\frac{1 + k_{20}}{2} + \frac{\mu(k_{10} + k_{20})}{2\alpha} \right)^2 - \mu k_{20} \right]^{\frac{1}{2}}. \quad (20)$$

Clearly, ρ_{LD} is independent of the exit rate parameter β . Eq. (16) provides us with N_1 in terms of ρ_{LD} , which has already been expressed in terms of the control parameters α , k_{10} , k_{20} , and μ of the model in Eq. (20). The PNC condition, which states $N_0 = N_1 + N_2 + L\rho_{LD}$ in the LD phase, can be used to find N_2 once N_1 has been obtained. Following are the expressions for N_1 and N_2 :

$$N_1 = L \frac{\mu}{\alpha} \rho_{LD}, \quad (21)$$

$$N_2 = L \left(\mu - \frac{\mu + \alpha}{\alpha} \rho_{LD} \right). \quad (22)$$

From Eq. (20), it can be seen that

$$\rho_{LD} \xrightarrow{\mu \rightarrow \infty} \frac{\alpha k_{20}}{k_{10} + k_{20}}. \quad (23)$$

We now investigate two special cases: one with equal particle exchange rates, i.e., $k_{10} = k_{20}$, and another when $k_{10} = 0, k_{20} \neq 0$. For the first case, ρ_{LD} goes to $\alpha/2$ as μ approaches ∞ , see Eq. (23). Substituting $\rho_{LD} = \alpha/2$ in the infinite- μ limit in Eqs. (21) and (22), we find $N_1 = N_0/2$ and $N_2 \approx N_0/2$. This implies, for infinitely large value of μ with equal particle exchange rates, majority of particles are accumulated in the reservoirs with almost equal proportion. For the second case when $k_{10} = 0$, ρ_{LD} approaches α as μ tends to ∞ , see Eq. (23). When substituted in Eqs. (21) and (22), $\rho_{LD} = \alpha$ gives $N_1 = N_0$ and $N_2 \approx 0$ in the infinite- μ limit. Thus, particles are mostly in reservoir R_1 with reservoir R_2 (and also the TASEP lane T) containing far fewer particles. The phase diagram of the model with $\mu \rightarrow \infty$ in the $\alpha - \beta$ plane is topologically identical to that of an open TASEP for all nonzero values of k_{10}, k_{20} .

We now determine the range of μ over which the LD phase can exist. For sufficiently small values of μ , there will certainly be an LD phase, the density of which will gradually rise with an increase in μ , as shown in Eq. (20). Eventually, ρ_{LD} approaches $\alpha k_{20}/(k_{10} + k_{20})$ as $\mu \rightarrow \infty$, as indicated in (23). Thus, the LD phase can be found for any value of μ in our model $0 \leq \mu < \infty$. This can be seen in the phase diagrams of Fig. 2, where LD phase appears for small values of μ ($\mu = 0.5$) as well as large values ($\mu = 100$).

Furthermore, the condition $\rho_{LD} < 1/2$ when imposed on Eq. (20) gives

$$\alpha < \left(\frac{k_{10} + k_{20}}{2k_{20} - \frac{1}{2} + k_{20}} \right). \quad (24)$$

This implies that, for a given set of values for k_{10}, k_{20} , and μ , the LD phase can only be obtained for α values satisfying the condition mentioned above. This is illustrated in the phase diagrams of Fig. 2. Consider, for example, the case with $k_{10} = 0, k_{20} = 0.95$, and $\mu = 1$ (upper right diagram), where the condition (24) indicates that the LD phase can exist only for $\alpha < 2.11$ according to MFT.

Fig. 2 gives the phase diagram of the present model for different values of μ with particle exchange rates $k_{10} = 0$ and $k_{20} = 0.95$. The LD phase is observed for all the values of μ , including large values such as $\mu = 100$.

B. High-density phase

The steady state bulk density in HD phase is given by

$$\rho_{HD} = 1 - \beta_{\text{eff}} = 1 - \beta \left(1 - \frac{N_2}{N_0} \right) > \frac{1}{2}. \quad (25)$$

Plugging N_2 obtained above in Eq. (14b) into Eq. (25) and using the expression for steady state current in the HD phase as $J_{HD} = \rho_{HD}(1 - \rho_{HD})$, we obtain a quadratic

equation in ρ_{HD} :

$$\rho_{HD} = 1 - \beta + \beta \left[\frac{k_1}{k_1 + k_2} \left(1 - \frac{\rho_{HD}}{\mu} \right) + \frac{\rho_{HD}(1 - \rho_{HD})}{N_0(k_1 + k_2)} \right]. \quad (26)$$

With $k_{1(2)} = k_{10(20)}/L$ in the weak coupling case and $N_0 = \mu L$, Eq. (26) translates into

$$\rho_{HD} = 1 - \beta + \beta \left[\frac{k_{10}}{k_{10} + k_{20}} \left(1 - \frac{\rho_{HD}}{\mu} \right) + \frac{\rho_{HD}(1 - \rho_{HD})}{\mu(k_{10} + k_{20})} \right], \quad (27)$$

solving which we get the following two solutions for ρ_{HD} :

$$\rho_{HD}^{\pm} = \left(\frac{1 - k_{10}}{2} - \frac{\mu(k_{10} + k_{20})}{2\beta} \right) \pm \left[\left(\frac{1 - k_{10}}{2} - \frac{\mu(k_{10} + k_{20})}{2\beta} \right)^2 + \frac{\mu k_{10}}{\beta} - \mu \left(1 - \frac{1}{\beta} \right) k_{20} \right]^{\frac{1}{2}}. \quad (28)$$

This has two solutions. Physically, in the limit when $N_2 \rightarrow 0$, any reservoir crowding effect ceases to operate and as a result $\beta_{\text{eff}} \rightarrow \beta$. Furthermore, in that case if there are infinite resources, i.e., $\mu \rightarrow \infty$, most of the particles are to be found in R_1 , giving $N_1 \approx N_0$ and $\alpha_{\text{eff}} \approx \alpha$. Such a situation can be achieved when $k_{10} = 0$ and $k_{20} \neq 0$ along with $\mu \rightarrow \infty$. We use these considerations to determine which of the two solutions in (28) is physically acceptable. Indeed, we find that between the two solutions of HD phase density in Eq. (28), the one with positive discriminant gives

$$\rho_{HD} \xrightarrow{\mu \rightarrow \infty} \left(1 - \frac{\beta k_{20}}{k_{10} + k_{20}} \right). \quad (29)$$

Thus, when $k_{10} = 0$, ρ_{HD} approaches $(1 - \beta)$ in the limit $\mu \rightarrow \infty$. This suggests the following as the HD phase density in the MFT:

$$\begin{aligned} \rho_{HD} &= \rho_{HD}^+ \\ &= \left(\frac{1 - k_{10}}{2} - \frac{\mu(k_{10} + k_{20})}{2\beta} \right) + \left[\left(\frac{1 - k_{10}}{2} - \frac{\mu(k_{10} + k_{20})}{2\beta} \right)^2 + \frac{\mu k_{10}}{\beta} - \mu \left(1 - \frac{1}{\beta} \right) k_{20} \right]^{\frac{1}{2}}. \end{aligned} \quad (30)$$

Unsurprisingly, ρ_{HD} is independent of α . To find the reservoir populations in the HD phase, we first obtain N_2 from Eq. (25) in terms of ρ_{HD} (expression of which is obtained in Eq. (30) in terms of model parameters), after which PNC relation $N_0 = N_1 + N_2 + L\rho_{HD}$ in the HD phase can be used to find N_1 . We thus find

$$N_1 = L \left[\frac{\mu(1 - \rho_{HD})}{\beta} - \rho_{HD} \right], \quad (31)$$

$$N_2 = L \left[\mu - \frac{\mu(1 - \rho_{HD})}{\beta} \right]. \quad (32)$$

As considered in our MFT for the LD phase above, we again analyse with two specific cases, $k_{10} = k_{20}$ and $k_{10} =$

0, $k_{20} \neq 0$, in the HD phase. For the first case, i.e., when $k_{10} = k_{20}$, Eq. (29) indicates that ρ_{HD} approaches $(1 - \beta/2)$ when $\mu \rightarrow \infty$. Consequently, substituting $\rho_{\text{HD}} = (1 - \beta/2)$ in Eqs. (31) and (32) when $\mu \rightarrow \infty$ yields $N_1 \approx N_0/2$ and $N_2 = N_0/2$. For the second case, i.e., when $k_{10} = 0, k_{20} \neq 0$, Eq. (29) gives ρ_{HD} approaching $(1 - \beta)$ in the limit of infinite- μ . Thus, substituting $\rho_{\text{HD}} = (1 - \beta)$ in Eqs. (31) and (32) when $\mu \rightarrow \infty$ results into $N_1 \approx N_0$ and $N_2 = 0$.

When μ is reduced, HD phase is less likely to occur due to insufficient supply of particles. Eventually, below a certain value of μ , HD phase will disappear. This lower threshold is determined later in Section V C. As $\mu \rightarrow \infty$, our model reduces to an open TASEP with $\rho_{\text{HD}} = 1 - \beta$ (for $k_{10} = 0, k_{20} \neq 0$), see Eq. (29). Thus, there will be no upper limit of μ for HD phase to occur. Using the fact $\rho_{\text{HD}} > 1/2$, one gets the following condition for HD phase existence:

$$\beta < \left(\frac{k_{10} + k_{20}}{2k_{20} + \frac{k_{10} - \frac{1}{2}}{\mu}} \right), \quad (33)$$

which implies that, for specific values of k_{10} , k_{20} , and μ , HD phase can occur when the condition mentioned above is satisfied. This is shown in the phase diagrams of Fig. 2. For instance, consider the case with $k_{10} = 0$, $k_{20} = 0.95$, and $\mu = 1$ (upper right phase diagram), where (33) suggests that the HD phase will exist for $\beta < 0.68$.

The phase diagrams in Fig. 2 illustrate the occurrence of the HD phase for different values of the parameter μ , specifically $\mu = 1$, $\mu = 1.5$, and $\mu = 100$. However, for $\mu = 0.5$, the phase diagram includes only the LD and DW phases.

C. Maximal current phase

The MC phase is characterised by $J_{\text{max}} = 1/4$ which is the maximum possible steady state particle current, and is obtained when the particle density $\rho = 1/2$ throughout the bulk of T [38]. Thus, in this phase, TASEP lane is half-filled and the PNC relation reads $N_0 = N_1 + N_2 + L/2$.

Analogous to an open TASEP, conditions for the existence of the MC phase in the present model are $\alpha_{\text{eff}} > 1/2$ and $\beta_{\text{eff}} > 1/2$. We determine the boundaries between the LD and MC phases, and between the HD and MC phases by setting $\rho_{\text{LD}} = 1/2$ and $\rho_{\text{HD}} = 1/2$ in Eqs. (20) and (30) respectively, which yields the following as LD-MC and HD-MC phase boundaries, respectively:

$$\alpha = \frac{\mu(k_{10} + k_{20})}{(2\mu - 1)k_{20} - \frac{1}{2}}, \quad (34)$$

$$\beta = \frac{\mu(k_{10} + k_{20})}{k_{10} + 2\mu k_{20} - \frac{1}{2}}. \quad (35)$$

Considering that α and β are non-negative real numbers in Eq. (34) and Eq. (35), we obtain

$$\mu > \mu_1 = \left(\frac{1}{2} + \frac{1}{4k_{20}} \right), \quad (36)$$

$$\mu > \mu_2 = \left(\frac{1}{4k_{20}} - \frac{k_{10}}{2k_{20}} \right). \quad (37)$$

Since $\mu_1 > \mu_2$ for any positive value of k_{10} and k_{20} , meeting (36) automatically infers fulfillment of (37). Thus the lower threshold of μ for MC phase existence is

$$\mu_i^{\text{MC}} = \left(\frac{1}{2} + \frac{1}{4k_{20}} \right). \quad (38)$$

This is also the lower threshold for HD phase existence, since if $\mu < \mu_i^{\text{MC}}$, the LD-MC phase boundary in Eq. (34) yields $\alpha < 0$, which is unphysical, thus ruling out the emergence of the HD phase in the phase diagram. This is shown in Fig. 2 for $\mu = 0.5$ (upper left phase diagram), where the exchange rate $k_{20} = 0.95$ yielding the lower threshold of μ for the existence of the MC and HD phases to be 0.76. As seen before, the present model reduces to an open TASEP in the limit $\mu \rightarrow \infty$. Thus, MC phase can be present for arbitrarily large values of μ as well. Taken together, following is the range within which MC and HD phases appear:

$$\left(\frac{1}{2} + \frac{1}{4k_{20}} \right) < \mu < \infty. \quad (39)$$

The phase diagrams of the model obtained by MFT and MCS with exchange rates $k_{10} = 0$ and $k_{20} = 0.95$ are shown in Fig. 2. The lower threshold for the existence of the MC phase is given by the condition (39) as $\mu = 0.76$ for these specific exchange rates, according to MFT. This prediction is confirmed by MCS simulations, where the MC phase does not exist for values of μ less than 0.76, such as $\mu = 0.5$.

D. Domain wall phase

In the DW phase, the density profile is piecewise continuous forming a DW that connects the LD and HD regions of a stationary density profile. Analogous to an open TASEP one has $\rho_{\text{LD}} = 1 - \rho_{\text{HD}} < 1/2$ in the DW phase. However, unlike in an open TASEP, the precise location of the DW in our model can be obtained by using PNC. Therefore, we get a localized domain wall (LDW), which is formed, say at a position x_w , in the bulk of the lane. The nonuniform bulk density in the DW phase can be represented in general as

$$\rho(x) = \rho_{\text{LD}} + \Theta(x - x_w)(\rho_{\text{HD}} - \rho_{\text{LD}}), \quad (40)$$

where ρ_{LD} and ρ_{HD} are the densities respectively in LD and HD domain of the DW and Θ is the Heaviside step function, defined as $\Theta(x) = 1$ for $x > 0$ and $\Theta(x) = 0$ for $x < 0$.

Particle number in T is given by

$$N_T = \sum_{i=1}^L \rho_i = L \int_0^1 \rho(x) dx. \quad (41)$$

Plugging $\rho(x)$ from Eq. (40) into Eq. (41), we get after simplifying

$$N_T = L \left[\alpha \frac{N_1}{N_0} (2x_w - 1) + 1 - x_w \right]. \quad (42)$$

Substituting N_T from Eq. (42) into the PNC relation, and the expression for the steady state current $J_{\text{DW}} = \rho_{\text{LD}}(1 - \rho_{\text{LD}})$ or $J_{\text{DW}} = \rho_{\text{HD}}(1 - \rho_{\text{HD}})$ in the DW phase into Eq. (14a), we obtain two equations coupled by N_1/N_0 and x_w :

$$\begin{aligned} \frac{N_1}{N_0} \left[\mu \left(1 - \frac{\alpha}{\beta} \right) + \alpha(2x_w - 1) \right] - x_w + 1 &= 0, \quad (43) \\ \frac{N_1}{N_0} &= \frac{k_2}{k_1 + k_2} \left[1 - \frac{1}{\mu} \left\{ \alpha \frac{N_1}{N_0} (2x_w - 1) + 1 - x_w \right\} \right] \\ &\quad - \frac{1}{N_0(k_1 + k_2)} \alpha \frac{N_1}{N_0} \left(1 - \alpha \frac{N_1}{N_0} \right). \end{aligned} \quad (44)$$

These equations provide two solutions for N_1/N_0 as follows:

$$\begin{aligned} \left(\frac{N_1}{N_0} \right)^\pm &= \left(\frac{1}{2\alpha} + \frac{\mu k_{10}}{2\alpha^2} + \frac{\mu k_{20}}{2\alpha\beta} \right) \\ &\quad \pm \left[\left(\frac{1}{2\alpha} + \frac{\mu k_{10}}{2\alpha^2} + \frac{\mu k_{20}}{2\alpha\beta} \right)^2 - \frac{\mu k_{20}}{\alpha^2} \right]^{\frac{1}{2}}, \end{aligned} \quad (45)$$

With these two possible solutions in Eq. (45), the density in the LD region of domain wall becomes

$$\begin{aligned} \rho_{\text{LD}} &= \alpha \left(\frac{N_1}{N_0} \right)^\pm \\ &= \left(\frac{1}{2} + \frac{\mu k_{10}}{2\alpha} + \frac{\mu k_{20}}{2\beta} \right) \\ &\quad \pm \left[\left(\frac{1}{2} + \frac{\mu k_{10}}{2\alpha} + \frac{\mu k_{20}}{2\beta} \right)^2 - \mu k_{20} \right]^{\frac{1}{2}}. \end{aligned} \quad (46)$$

At the LD-DW phase boundary, the density corresponding to the LD phase [Eq. (20)] must be identical to the acceptable density in the LD part of domain wall [Eq. (46)]. Considering the solution of Eq. (46) with negative discriminant, we found that it is identical to the LD phase density given in Eq. (20) under the following condition:

$$\mu \left(1 - \frac{\alpha}{\beta} \right) + \alpha = 0. \quad (47)$$

Eq. (47) is exactly the same equation that defines the boundary between LD and DW phases, which we will

obtain later [Eq. (56)] in another way. Thus the acceptable solution for N_1/N_0 is

$$\begin{aligned} \frac{N_1}{N_0} &= \left(\frac{1}{2\alpha} + \frac{\mu k_{10}}{2\alpha^2} + \frac{\mu k_{20}}{2\alpha\beta} \right) \\ &\quad - \left[\left(\frac{1}{2\alpha} + \frac{\mu k_{10}}{2\alpha^2} + \frac{\mu k_{20}}{2\alpha\beta} \right)^2 - \frac{\mu k_{20}}{\alpha^2} \right]^{\frac{1}{2}}. \end{aligned} \quad (48)$$

In the DW phase

$$\rho_{\text{LD}} + \rho_{\text{HD}} = 1, \quad (49)$$

$$\implies \alpha_{\text{eff}} = \beta_{\text{eff}}, \quad (50)$$

$$\implies \alpha \frac{N_1}{N_0} = \beta \left(1 - \frac{N_2}{N_0} \right). \quad (51)$$

One then gets the expression of N_2 from that of N_1 :

$$\begin{aligned} \frac{N_2}{N_0} &= 1 - \frac{\alpha}{\beta} \frac{N_1}{N_0} \\ &= 1 - \left(\frac{1}{2\beta} + \frac{\mu k_{10}}{2\alpha\beta} + \frac{\mu k_{20}}{2\beta^2} \right) \\ &\quad + \left[\left(\frac{1}{2\beta} + \frac{\mu k_{10}}{2\alpha\beta} + \frac{\mu k_{20}}{2\beta^2} \right)^2 - \frac{\mu k_{20}}{\beta^2} \right]^{\frac{1}{2}}. \end{aligned} \quad (52)$$

Consequently, the DW position (x_w) is obtained by solving Eq. (43). We obtain

$$x_w = \frac{1 - \frac{N_1}{N_0} \left[\mu \left(\frac{\alpha}{\beta} - 1 \right) + \alpha \right]}{1 - 2\alpha \frac{N_1}{N_0}}. \quad (53)$$

Substituting N_1/N_0 from Eq. (48) into Eq. (53), one finds x_w in terms of the control parameters, α , β , μ , k_{10} , and k_{20} , of the model. Furthermore, densities corresponding to the LD and HD regions of the DW phase can be calculated as follows:

$$\begin{aligned} \rho_{\text{LD}} &= \alpha \frac{N_1}{N_0} \\ &= \left(\frac{1}{2} + \frac{\mu k_{10}}{2\alpha} + \frac{\mu k_{20}}{2\beta} \right) \\ &\quad - \left[\left(\frac{1}{2} + \frac{\mu k_{10}}{2\alpha} + \frac{\mu k_{20}}{2\beta} \right)^2 - \mu k_{20} \right]^{\frac{1}{2}}, \end{aligned} \quad (54)$$

with $\rho_{\text{HD}} = 1 - \rho_{\text{LD}}$. The DW height (Δ) is then

$$\begin{aligned} \Delta &= \rho_{\text{HD}} - \rho_{\text{LD}} \\ &= \left[\left(1 + \frac{\mu k_{10}}{\alpha} + \frac{\mu k_{20}}{\beta} \right)^2 - 4\mu k_{20} \right]^{\frac{1}{2}} - \left(\frac{\mu k_{10}}{\alpha} + \frac{\mu k_{20}}{\beta} \right). \end{aligned} \quad (55)$$

To determine the boundaries between the LD as well as the HD and DW phases, we make use of the fact that the domain wall is situated at the far right and left ends of the TASEP lane at the point of LD-DW and HD-DW transitions, respectively. By setting $x_w = 1$ and $x_w = 0$

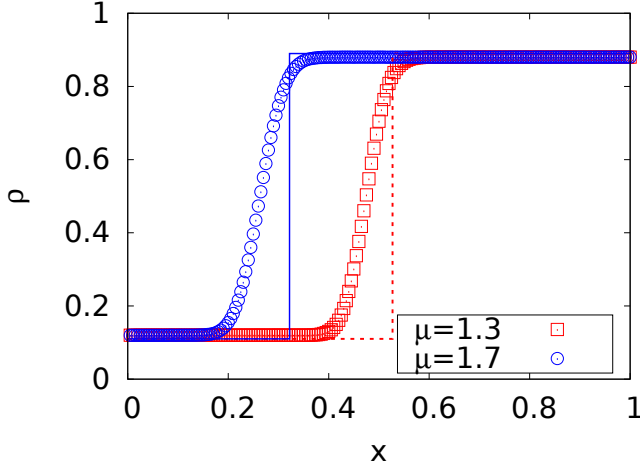


FIG. 3: Plot of an LDW in the weak coupling limit of the model. System size is $L = 1000$ and 2×10^9 Monte Carlo steps are performed to get the density profiles. Lines (solid and dotted) represent the MFT predictions, whereas discrete points are the MCS results. For smaller values of μ we get an LDW. Two different sets of parameters are chosen: $\alpha = 0.2$, $\beta = 0.12$, $\mu = 1.3$, $k_{10} = 0$, and $k_{20} = 0.95$ (red); $\alpha = 0.2$, $\beta = 0.12$, $\mu = 1.7$, $k_{10} = 0$, and $k_{20} = 0.95$ (blue). Clearly, increasing the value of μ shifts the LDW position to the left [see Eq. (53)].

in Eq. (53), we obtain the following equations that define the LD-DW and HD-DW phase boundaries respectively:

$$\mu \left(1 - \frac{\alpha}{\beta}\right) + \alpha = 0, \quad (56)$$

$$\frac{N_1}{N_0} \left[\mu \left(1 - \frac{\alpha}{\beta}\right) - \alpha \right] + 1 = 0, \quad (57)$$

with N_1/N_0 given in Eq. (48). The DW position x_w obtained in Eq. (53) spans from 0 to 1 with $x_w = 0$ and $x_w = 1$ corresponding to the HD-DW and LD-DW phase boundaries, respectively. Analogous to the open TASEP, the DW phase in the present model is characterised by $\alpha_{\text{eff}} = \beta_{\text{eff}} < 1/2$. Since $\alpha_{\text{eff}} = \alpha N_1/N_0 < 1/2$, the denominator in Eq. (53) is always positive. The condition $x_w > 0$ then is met only if the numerator in Eq. (53) is positive, which leads to

$$\mu \left(1 - \frac{\alpha}{\beta}\right) > \alpha - \frac{N_0}{N_1}. \quad (58)$$

Also, the condition $x_w < 1$ when applied in Eq. (53) yields the following:

$$\mu \left(1 - \frac{\alpha}{\beta}\right) < -\alpha. \quad (59)$$

Within the DW phase, the right-hand side of (58), $\alpha - N_0/N_1$, is negative. Moreover, the right-hand side of (59) is clearly negative (α being positive always) indicating the left-hand side, $\mu(1 - \alpha/\beta)$, to be negative. Given

$\mu > 0$, this implies $(1 - \alpha/\beta)$ to be negative or $\alpha > \beta$ over the DW region. We recast these inequalities (58) and (59) as follows:

$$\mu \left(\frac{\alpha}{\beta} - 1\right) < \frac{N_0}{N_1} - \alpha, \quad (60)$$

$$\mu \left(\frac{\alpha}{\beta} - 1\right) > \alpha. \quad (61)$$

Taken together, (60) and (61) delineate the range of μ within which the DW phase exists:

$$\left(\frac{\alpha}{\beta} - 1\right) < \mu < \left(\frac{\frac{N_0}{N_1} - \alpha}{\frac{\alpha}{\beta} - 1}\right). \quad (62)$$

The thresholds of μ for DW phase existence obtained in (62) are not fixed but can be varied with the control parameters involved. Only the region in the $\alpha - \beta$ plane for a given μ that satisfies *both* (60) and (61) simultaneously admits an LDW. Notice that the line $\alpha = \beta$ satisfies (60) but not (61), meaning the line $\alpha = \beta$ falls *outside* the DW phase region in the phase diagram. From (60) and (61), we find that as μ approaches infinity, both LD-DW and HD-DW boundaries converge to the $\alpha = \beta$ line, which is below them for any finite μ ; see the phase diagrams in Fig. 2.

See Fig. 3 for stationary densities in the form of LDWs. In MFT, PNC gives a solution for the position x_w of the DW, corresponding to an LDW. However, our results from the MCS studies reveal that for smaller values of μ , an LDW is obtained, whereas for larger values of μ , the DW gets delocalized. We attribute this to fluctuations; see Section VII below for additional results and discussions.

Our MCS studies reveal that increasing the particle number causes them being accumulated near the entrance end of T , thus positioning the DW towards left side. This is illustrated in Fig. 4 (left), where x_w is observed to decrease with increasing μ . The DW height Δ , however, remains nearly unchanged with varying μ , see Fig. 4 (right). In Fig. 5, the variation of x_w and Δ with k_{20} for a fixed value of μ is shown.

E. Phase boundaries meet at a common point

Within a specific range of μ where all four phases can be present in the $\alpha - \beta$ plane, the phase boundaries converge at a common point known as the (four-phase) *multicritical point*. This is the point where four phase boundaries [see Eqs. (34), (35), (56), and (57)] intersect:

$$(\alpha_c, \beta_c) = \left(\frac{\mu(k_{10} + k_{20})}{(2\mu - 1)k_{20} - \frac{1}{2}}, \frac{\mu(k_{10} + k_{20})}{k_{10} + 2\mu k_{20} - \frac{1}{2}} \right). \quad (63)$$

Thus (α_c, β_c) depends explicitly on k_{10} , k_{20} , and μ . In the limit $\mu \rightarrow \infty$, the multicritical point approaches

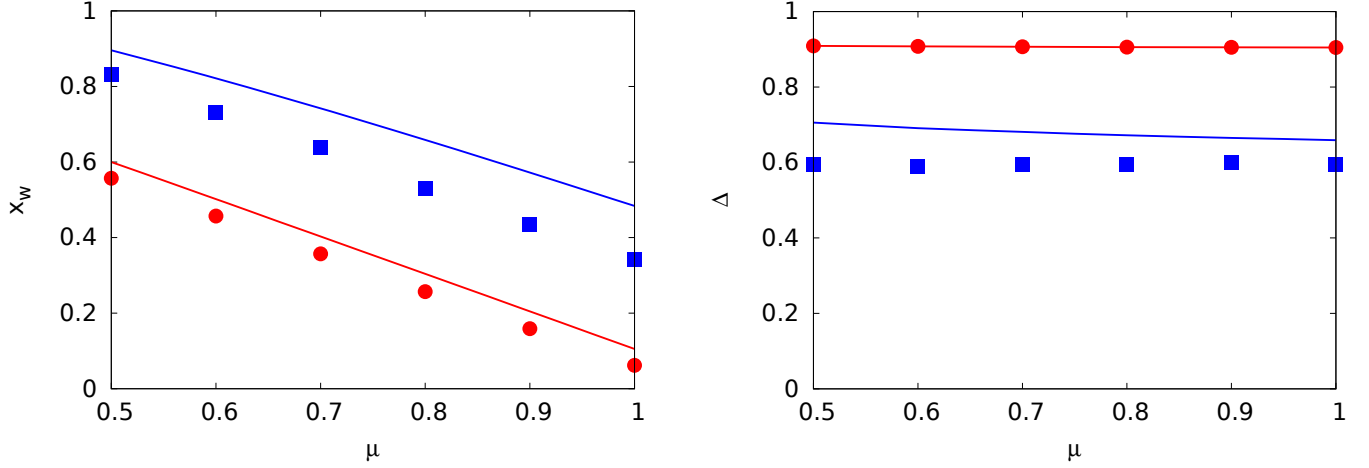


FIG. 4: **(Left)** Plots of x_w vs. μ in the weak coupling limit, with parameter values: $\alpha = 0.5$, $\beta = 0.05$, $k_{10} = 0$, and $k_{20} = 0.95$ (red); $\alpha = 0.5$, $\beta = 0.2$, $k_{10} = 0$, and $k_{20} = 0.95$ (blue). Solid lines depict MFT results, while discrete points show MCS results. MFT and MCS agree better for lower parameter values, as seen in the first red set. **(Right)** Plots of Δ vs. μ in the weak coupling limit using the same parameter values as in the left figure. These plots demonstrate that the DW position x_w diminishes as μ increases [see Eq. (53)], whereas the DW height Δ remains relatively constant with changes in μ [see Eq. (55)].

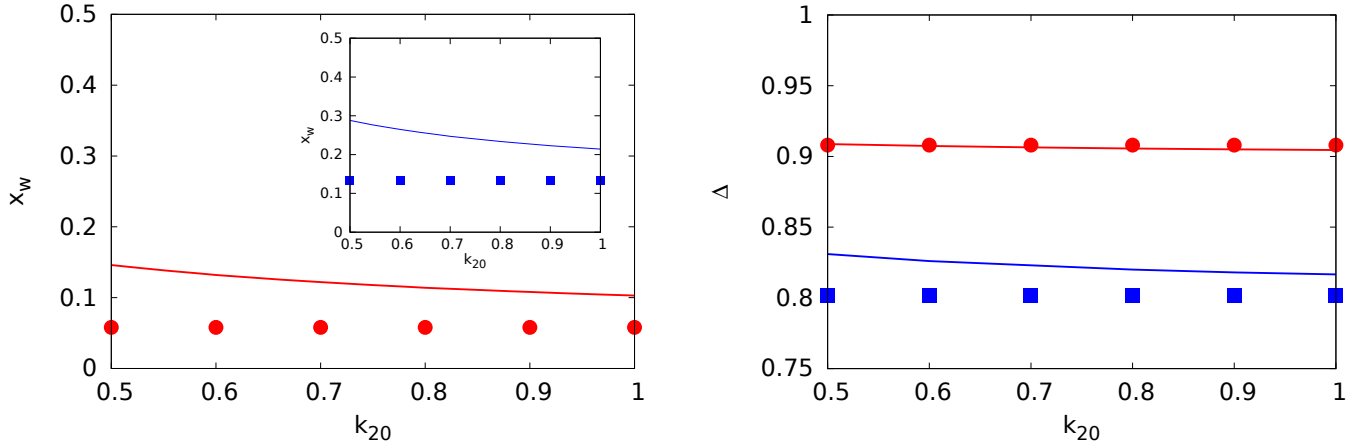


FIG. 5: **(Left)** Plots of x_w vs. k_{20} in the weak coupling limit. Parameter values are: $\alpha = 0.5$, $\beta = 0.05$, $\mu = 1$, and $k_{10} = 0$ for the main plot (red); $\alpha = 0.5$, $\beta = 0.1$, $\mu = 1$, and $k_{10} = 0$ for the inset plot (blue). **(Right)** Plots of Δ vs. k_{20} in the weak coupling limit. Parameter values are same as the left figure. MFT results [see Eq. (53) and (55)] are shown as solid lines, while MCS outcomes are depicted as discrete points.

$$(\alpha_c, \beta_c)_{\mu \rightarrow \infty} = \left(\frac{k_{10} + k_{20}}{2k_{20}}, \frac{k_{10} + k_{20}}{2k_{20}} \right). \quad (64)$$

Thus, for $k_{10} = k_{20}$, $(\alpha_c, \beta_c)_{\mu \rightarrow \infty} = (1, 1)$ and for $k_{10} = 0, k_{20} \neq 0$ we have $(\alpha_c, \beta_c)_{\mu \rightarrow \infty} = (1/2, 1/2)$. Clearly from (63) this multicritical point exists for

$$\mu > \left(\frac{1}{2} + \frac{1}{4k_{20}} \right), \quad (65)$$

which is the lower threshold of μ for MC phase existence; see the condition (39).

The distance d between the origin (0,0) and the mul-

ticritical point (α_c, β_c) is calculated as

$$d = \sqrt{\left(\frac{\mu(k_{10} + k_{20})}{(2\mu - 1)k_{20} - \frac{1}{2}} \right)^2 + \left(\frac{\mu(k_{10} + k_{20})}{k_{10} + 2\mu k_{20} - \frac{1}{2}} \right)^2}. \quad (66)$$

This implies that the distance d diverges as μ approaches the threshold $(1/2 + 1/4k_{20})$ from above. We get

$$d \xrightarrow{\mu \rightarrow \infty} \frac{k_{10} + k_{20}}{\sqrt{2}k_{20}}. \quad (67)$$

Consequently for $k_{10} = k_{20}$ one gets $d \rightarrow \sqrt{2}$, while $d \rightarrow 1/\sqrt{2}$ when $k_{10} = 0, k_{20} \neq 0$.

F. NATURE OF THE PHASE TRANSITIONS

As shown in Fig. 2, the phase diagrams in weak coupling limit of the present model are markedly different from that for an open TASEP. This is attributed to the global particle number conservation and dynamically controlled effective entry and exit rates for the TASEP channel. Depending on the values of μ , there are either two or four phases in the $\alpha - \beta$ plane; see Fig. 2. We now briefly discuss the nature of the phase transitions. As in an open TASEP, we consider the steady state bulk density (ρ) as the order parameter. We recall that in open TASEP, the transition between LD and HD phases is marked by a sudden jump in ρ , thus implying it a first-order phase transition. On the other hand, the transitions between either LD or HD phases and the MC phase involve continuous changes in ρ , indicative of second-order phase transitions. In the present model, there are *no* phase transitions between the LD and HD phases for any finite μ . Instead, there are transitions from the LD to

A significant deviation, particularly for small and intermediate values of μ , between our analytical mean-field and simulated Monte Carlo results has been observed in the weak coupling limit of the model; see Fig. 2, Fig. 3, Fig. 4, Fig. 5, Fig. 7, and Fig. 8. In contrast, we have observed excellent agreement between MFT and MCS results in the strong coupling case, see Fig. 9, Fig. 10, Fig. 11, Fig. 12, and Fig. 14 in the Appendix. This Section explains the reason behind such discrepancies. The argument is similar to a recent study on a similar model consisting of a single TASEP lane connected to two reservoirs at both its ends [33] except for large μ -values where the present model reduces to an open TASEP model. MFT often produces satisfactory outcomes as long as the fluctuation effects can be neglected.

In Fig. 7, discrepancies between MFT predictions and MCS results in steady state density profiles in the weak coupling limit are shown for a set of control parameters mentioned in the caption. With parameters specified in the left plot, MFT suggest an LD phase with density $\rho_{LD} = 0.44$, while MCS suggests an MC phase. In the center plot, MFT predicts an LDW, whereas MCS yields HD phase with density $\rho_{HD} = 0.69$. In the right plot, both MFT and MCS suggest occurrence of an LDW but with different densities and positions. The system size is $L = 1000$ and time-average with 2×10^9 (red circles) and 2×10^{10} (blue squares) number of runs are performed. No indication of improvement between theoretical and simulative results in the density profiles are observed. We now argue for these discrepancies.

We now set up heuristic arguments to explain the fluctuation-induced disagreements between the MFT and MCS results in the thermodynamic limit by following and extending the arguments developed in Ref. [33]. Fluctu-

ation induces deviations in the effective value of reservoir populations from their respective MFT values. One can thus generalise the relations $\alpha_{\text{eff}} = \alpha N_1/N_0$ and $\beta_{\text{eff}} = \beta(1 - N_2/N_0)$ to

In Fig. 6, we show the variation of the reservoir population ratio (N_1/N_2) with respect to either μ with constant exchange rates or the ratio of exchange rates (k_{10}/k_{20}) with a fixed μ in the weak coupling limit in the LD phase, see Eqs. (20), (21), and (22). Discrepancies between MFT and MCS results are clearly visible in some cases.

VI. ROLE OF FLUCTUATIONS

ation induces deviations in the effective value of reservoir populations from their respective MFT values. One can thus generalise the relations $\alpha_{\text{eff}} = \alpha N_1/N_0$ and $\beta_{\text{eff}} = \beta(1 - N_2/N_0)$ to

$$\tilde{\alpha}_{\text{eff}} = \frac{\alpha}{N_0} N_1^{\text{eff}}, \quad \tilde{\beta}_{\text{eff}} = \beta \left(1 - \frac{N_2^{\text{eff}}}{N_0} \right) \quad (68)$$

with

$$N_1^{\text{eff}} = N_1 + \delta N_1, \quad N_2^{\text{eff}} = N_2 + \delta N_2, \quad (69)$$

where N_1, N_2 are the solution for the populations of reservoirs R_1, R_2 in MFT [i.e., solutions in Eqs. (15a) and (15b)], $\delta N_1, \delta N_2$ are the corresponding deviations due to the fluctuations from their respective mean-field values, and $\tilde{\alpha}_{\text{eff}}, \tilde{\beta}_{\text{eff}}$ are the effective entry, exit rates in MCS studies. Since δN_1 and δN_2 are fluctuations, they can be positive or negative, making $\tilde{\alpha}_{\text{eff}} - \alpha_{\text{eff}}$ and $\beta_{\text{eff}} - \tilde{\beta}_{\text{eff}}$ positive or negative accordingly.

In the weak coupling limit, as shown in Eqs. (15a) and (15b), N_1 and N_2 have dependence on TASEP current J_T that scales as LJ_T . J_T being a bounded quantity ($J_{T_{\text{max}}} = 1/4$), fluctuation in J_T is $\mathcal{O}(1)$. Hence the reservoir populations N_1, N_2 as well as their fluctuations $\delta N_1, \delta N_2$ must be $\mathcal{O}(L)$ quantities. Indeed, the ratio of N_1, N_2 depends explicitly on J_T . This immediately gives $\tilde{\alpha}_{\text{eff}} - \alpha_{\text{eff}} \sim \mathcal{O}(1)$ and $\beta_{\text{eff}} - \tilde{\beta}_{\text{eff}} \sim \mathcal{O}(1)$ even in the thermodynamic limit. Furthermore, the sum of the two reservoir populations $N_R = N_0 - N_T$ should scale with L (for a fixed μ) and hence should have typical fluctuations of the size $\mathcal{O}(\sqrt{N_R}) \sim \mathcal{O}(\sqrt{L}) \ll$ fluctuations in N_1 or N_2 in the limit of large L . Given that $N_1 + N_2 = N_R$, we must have $\delta N_1 \sim -\delta N_2$ to the leading order in L for sufficiently large L . This in turn means when N_1^{eff}

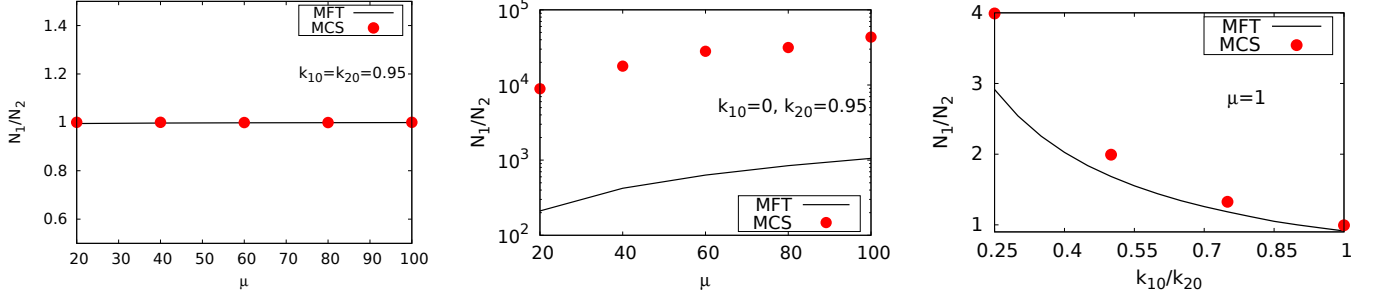


FIG. 6: Plot of the reservoir population ratio N_1/N_2 versus μ in the weak coupling limit of the model for fixed (**Left**) $k_{10} = k_{20} = 0.95$ with good agreement between MFT and MCS visible, (**Middle**) $k_{10} = 0, k_{20} = 0.95$ with discrepancies between MFT and MCS results visible. (**Right**) Plot of N_1/N_2 with k_{10}/k_{20} for $\mu = 1$ in the weak coupling limit. In these plots, the entry and exit rates are carefully selected to ensure that the TASEP lane remains only in one phase (which is here the LD phase). The values of $\alpha = 0.1$ and $\beta = 1$ are used. Notice the mismatches between MFT and MCS results increasing with decreasing k_{10}/k_{20} . MFT results in these plots are obtained from Eqs. (20), (21), and (22).

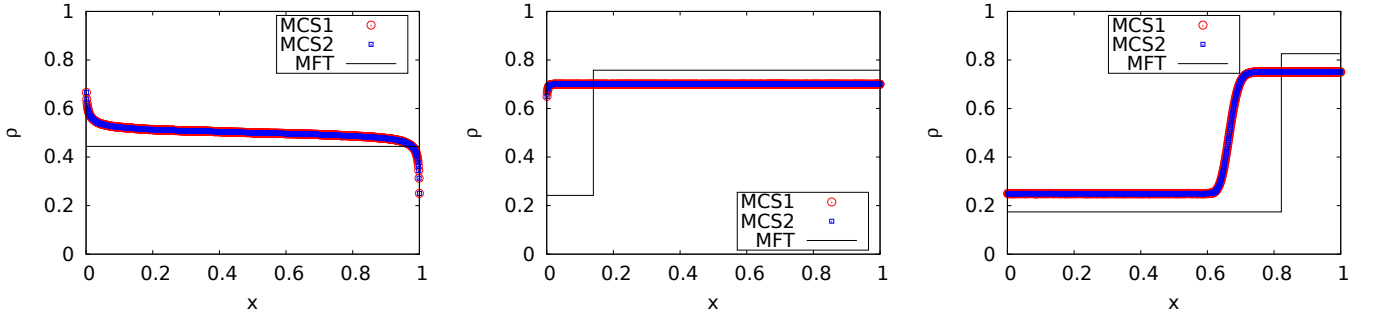


FIG. 7: Disagreements in the MFT and MCS results on the density profiles in the weak coupling limit of the model. Solid line represents MFT predictions (see Sections VA, VB, VC, and VD) while discrete points show MCS results. Two sets of MCS results, labeled as MCS1 (red circles) and MCS2 (blue squares), correspond to time-averaged densities with 2×10^9 and 2×10^{10} runs, respectively. Notably, fluctuations persist even for longer runs. The system size is fixed at $L = 1000$. (**Left**) For parameters $\alpha = 1.5$, $\beta = 1.2$, $\mu = 1$, $k_{10} = 0$, and $k_{20} = 0.95$, MFT predicts an LD phase with density $\rho_{LD} = 0.44$, while MCS suggests an MC phase with density $\rho_{MC} = 0.5$. (**Middle**) In the case of $\alpha = 2$, $\beta = 0.3$, $\mu = 1$, $k_{10} = 0$, and $k_{20} = 0.95$, MFT and MCS predict DW and HD phases (with density $\rho_{HD} = 0.69$), respectively. (**Right**) With parameters $\alpha = 1.5$, $\beta = 0.25$, $\mu = 0.5$, $k_{10} = 0$, and $k_{20} = 0.95$, both MFT and MCS predict a DW phase. However, MFT suggests an LDW with different low and high densities and positions compared to MCS. See text in Section VI.

is larger (smaller) than N_1 , N_2^{eff} is smaller (larger) than N_2 , giving $\tilde{\alpha}_{\text{eff}} > (<) \alpha_{\text{eff}}$ and $\tilde{\beta}_{\text{eff}} > (<) \beta_{\text{eff}}$. This suggests that in the weak coupling case, fluctuations persist in the thermodynamic limit, causing the transition between LD or HD phases to occur at values of α and β distinct from those predicted by MFT. Contrastingly, in the strong coupling regime, N_1 and N_2 become independent of J_T in the thermodynamic limit and are found to maintain a fixed ratio, $N_1/N_2 = k_2/k_1$, see Appendix. The particle exchange dynamics between reservoirs effectively resemble equilibrium dynamics, leading to δN_1 and δN_2 scaling as $\mathcal{O}(\sqrt{L})$. As the MF expressions for N_1 and N_2 scale with L , in the thermodynamic limit, $\tilde{\alpha}_{\text{eff}} \rightarrow \alpha_{\text{eff}}$ and $\tilde{\beta}_{\text{eff}} \rightarrow \beta_{\text{eff}}$. This convergence ensures a strong quantitative agreement between MFT and MCS results in the strong coupling case.

Interestingly, the phase diagrams in both weak and strong coupling limit reveals that MFT and MCS results

are in excellent agreement for large values of μ , see Fig. 2 ($\mu = 100$) and Fig. 9 ($\mu = 1000$). This is argued below. With $N_0 = \mu L$, Eq. (68) leads to

$$\tilde{\alpha}_{\text{eff}} = \frac{\alpha(N_1 + \delta N_1)}{N_0} = \alpha_{\text{eff}} + \frac{1}{\mu} \frac{\alpha \delta N_1}{L}, \quad (70)$$

$$\tilde{\beta}_{\text{eff}} = \beta \left(1 - \frac{N_2 + \delta N_2}{N_0} \right) = \beta_{\text{eff}} - \frac{1}{\mu} \frac{\beta \delta N_2}{L}, \quad (71)$$

where entry and exit rates *with* and *without* tilde corresponds to MCS and MFT respectively. As $\delta N_1, \delta N_2$ are $\mathcal{O}(L)$ quantities in the weak coupling limit, fluctuations in the MCS values of entry and exit rates (second part of Eqs. (70) and (71)) are clearly $\mathcal{O}(1/\mu)$ quantities that vanishes in the limit $\mu \rightarrow \infty$, thereby giving $\tilde{\alpha}_{\text{eff}} \rightarrow \alpha_{\text{eff}}$ and $\tilde{\beta}_{\text{eff}} \rightarrow \beta_{\text{eff}}$ in the thermodynamic limit.

VII. DELOCALIZATION OF THE LDW

We have discussed above the conditions to form LDWs in the weak coupling limit of the model in the mean-field theory. The MFT predicts unique LDW positions [see Eq. (53)], which can be evaluated by using PNC. For low values of μ , the MFT agrees qualitatively with the MCS results, as can be seen in Fig. 3. However, as mentioned above, for large values of μ , the LDW clearly delocalizes; see Fig. 8 (top); see also Fig. 13 (left). More intriguingly, for $k_{10} \gg k_{20}$, the tendency to delocalize vanishes even with very large values of μ ; see Fig. 8 (bottom). We now explore these systematically below by using our analysis in Section VI above.

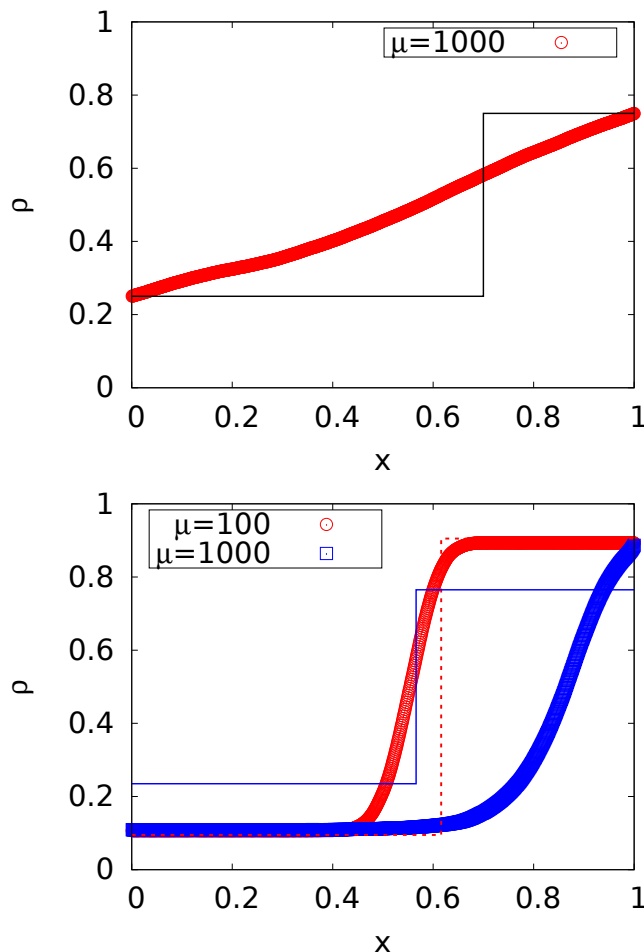


FIG. 8: Plots of domain walls in the weak coupling limit of the model with system size $L = 1000$. **(Top)** Increasing μ sufficiently (of the order of L), we can get DDW for some choices of the particle exchange rates. Parameter values are: $\alpha = 0.25$, $\beta = 0.2499$, $\mu = 1000$, $k_{10} = 0$, and $k_{20} = 0.95$. **(Bottom)** Parameter values: $\alpha = 10$, $\beta = 7$, $\mu = 100$, $k_{10} = 0.95$, and $k_{20} = 0.01$ (red); $\alpha = 23$, $\beta = 22$, $\mu = 1000$, $k_{10} = 0.95$, and $k_{20} = 0.01$ (blue). With these sets of parameter values where $k_{10} \gg k_{20}$, only LDWs are formed even with very large values of μ ; see text in Section VII.

We have in general, $N_1, N_2 \sim \mathcal{O}(\mu L)$. This means typical fluctuations in $N_1, N_2 \sim \mathcal{O}(\sqrt{\mu L})$. Now, for a single DDW-like domain wall to exist in TASEP lane, domain wall position x_w must fluctuate over a scale comparable to L , which gives a typical number fluctuation in TASEP as $\mathcal{O}(L)$. Number conservation implies number fluctuations in the TASEP must be the same as the number fluctuations in N_1, N_2 . This means that fluctuations in N_1 and $N_2 \sim \mathcal{O}(L)$, for a DDW to exist, which immediately gives $\mu \sim L$ for DDW to occur [11]. Our MCS results in Fig. 8 (top) satisfies this. We however note that Fig. 8 (bottom) *is not* a DDW, in spite of having a large μ . This can be explained by considering the Fokker-Planck equation for the probability P to find the DW at a point x_w in the bulk [12, 34, 39], which has the form

$$\frac{\partial P}{\partial t} = D \frac{\partial^2 P}{\partial x^2}. \quad (72)$$

Here, $D \equiv [\alpha_{\text{eff}}(1 - \alpha_{\text{eff}}) + \beta_{\text{eff}}(1 - \beta_{\text{eff}})]$ is the diffusivity. For a DW, $\alpha_{\text{eff}} = \beta_{\text{eff}}$, which for Fig. 8(bottom) become very small. This means the typical time-scale for the DW to span the entire TASEP channel due to fluctuations becomes very large, which effectively localizes the DW. This explains an LDW in Fig. 8(bottom).

VIII. CONCLUSIONS AND OUTLOOK

In this work, we have studied the generic nonequilibrium steady state density profiles and phase diagrams of a quasi-1D current-carrying channel T connecting two particle reservoirs R_1 and R_2 with unlimited storage capacity. Particles from the left reservoir R_1 enter the channel T , followed by a unidirectional (from left to right) hopping throughout T subject to exclusion and eventually reach the right reservoir R_2 . To model diffusion in our system, the reservoirs are allowed to exchange particles directly between them. The later process ensures a finite current, making it essentially a nonequilibrium system to study. In this model, entry and exit of particles into and from the lattice are dynamically controlled by the instantaneous population of reservoirs, unlike the open TASEP where these two rates are constant and uncorrelated. In this model, there is no upper bound for the total particle number that is held conserved by the dynamics. This sets our model apart from the particle nonconserving dynamics of open TASEP. Actual or effective entry and exit rates in our model are controlled by the parameters α and β , together with the two functions f and g . We choose simple forms of f and g , see Eq. (3), where f and g respectively are the monotonically increasing and decreasing functions of N_1 and N_2 with values between 0 and 1, N_1 and N_2 being the populations of reservoirs R_1 and R_2 . Taken together, the dynamics of the system is influenced by five control parameters – one entry and exit rate (α and β), two particle exchange rates (k_1 and k_2), and a filling fraction μ . The behaviour of the system is particularly interesting when particle hopping

through the lattice sites and direct particle exchange between the reservoirs compete. This corresponds to the *weak coupling limit*, captured by scaling k_1 and k_2 with $\mathcal{O}(1/L)$, where L represents the lattice size. We have also studied the *strong coupling limit*, where direct particle exchange between reservoirs dominates particle current through TASEP lane, i.e., $k_1, k_2 \sim \mathcal{O}(1)$.

We have analysed our model at the mean-field level and corroborated the MFT analytical results with Monte Carlo simulations. Depending on the value of μ , generally either two or four phases appear simultaneously in the $\alpha - \beta$ phase plane, with continuous transitions between them. Above a lower threshold of μ , all these phases meet at a single point. Interestingly, in the limit of infinite μ , the phase diagram of our model mimics that of an open TASEP. Indeed, when $\mu \rightarrow \infty$, the phase space of the present model includes three phases – LD, HD, and MC — with a DW region in the form of an inclined line connecting LD phase to the HD phase. Initially manifested as localized domain walls (LDWs) for smaller μ values, these are now delocalized domain walls (DDW) in this limit. While PNC together with MFT still predicts an LDW, large fluctuations around the mean-field position of the DW effectively delocalizes the domain wall, giving a DDW.

It is useful to compare our results with a recent work on a similar model with one TASEP lane connected to two reservoirs directly exchanging particles that uses different forms for the functions f and g , Ref. [33]. First of all, the model in Ref. [33] has a particle-hole symmetry for equal exchange rates between the reservoirs in both weak and strong coupling limits. In contrast, in the present model, there is none. As mentioned in the Introduction Section, in the model of Ref. [33], the maximum particle content is limited by the exchange rates between the reservoirs: Consequently, μ in the model of Ref. [33] can have a maximum value $\mu_{\max} = (2 + k_{20}/k_{10})$. In contrast, in the model of the present study, it is independent or free of any other model parameters. Thus the present model has less constraints. In addition, the model in Ref. [33], admits particle-hole symmetry in the special case of equal exchange rates, i.e., $k_1 = k_2$, unlike for the present model that has no particle-hole symmetry for any choice of the model parameters. In contrast to the model in Ref. [33], for any finite values of the exchange rates, the DW in the present model can delocalize if sufficiently large number of particles are available. This leads to the significant differences in the phase diagrams in the two models for large “resources” or large number of particles, i.e., for large values of μ . Unsurprisingly, for fewer particles, i.e., for small μ , the differences in the phase diagrams are small. On the whole, our studies here together with Ref. [33] reveal how the presence or absence of constraints on the dynamics of the models can strongly influence the stationary densities and the phase diagrams.

We have used analytical MFT, supplemented by extensive studies to obtain the stationary densities and the

phase diagrams. In the weak coupling limit, we find significant disagreements between the MFT and MCS results for intermediate values of μ . Such disagreements disappear in the strong coupling limit of the model. We further find that the domain wall can delocalize for some choices of k_{10}, k_{20} , but does not delocalize for other choices even for sufficiently larger values of μ . We are able to explain these results in terms of a set of heuristic arguments that show the crucial role of fluctuations that survive in the thermodynamic limit in the weak coupling limit, but not in the strong coupling case.

Our studies can be extended in various ways. One can consider several TASEP lanes connecting the two reservoirs. More interestingly, one can consider a “mixed model”, where one of the reservoirs has the structure of the reservoirs in Ref. [33], and the other has a form similar to the present study. This can lead to possible unexpected competitions between the reservoir structures and the resulting phase diagrams. We hope our studies here will stimulate further research along these lines.

IX. ACKNOWLEDGEMENT

A.B. thanks SERB (DST), India for partial financial support through the CRG scheme [file: CRG/2021/001875].

Appendix A: STRONG COUPLING LIMIT

In this Section, we focus on the strong coupling limit of the model, and study the phase diagrams and density profiles. The strong coupling limit is characterised by the particle exchange rates independent of system size L , i.e., $k_1, k_2 \sim \mathcal{O}(1)$. This means the direct exchange of particles between reservoirs dominates over the particle transport via hopping through the TASEP. Therefore, in this limit, the reservoir populations N_1 and N_2 maintain a fixed ratio for a given set of particle exchange rates. This considerably simplifies the corresponding MFT calculations, which agrees quantitatively with the MCS results, contrasting the weak coupling limit.

1. Mean-field phase diagrams and steady state densities

Phase diagrams in the strong coupling limit are shown in Fig. 9 for a set of representative values of μ with $k_1 = 0$ and $k_2 = 0.95$. As explained in Section III above, in the strong coupling limit

$$\frac{N_1}{N_2} = \frac{k_2}{k_1} \quad (\text{A1})$$

in the thermodynamic limit ($L \rightarrow \infty$). To calculate the steady state densities in the different phases in the

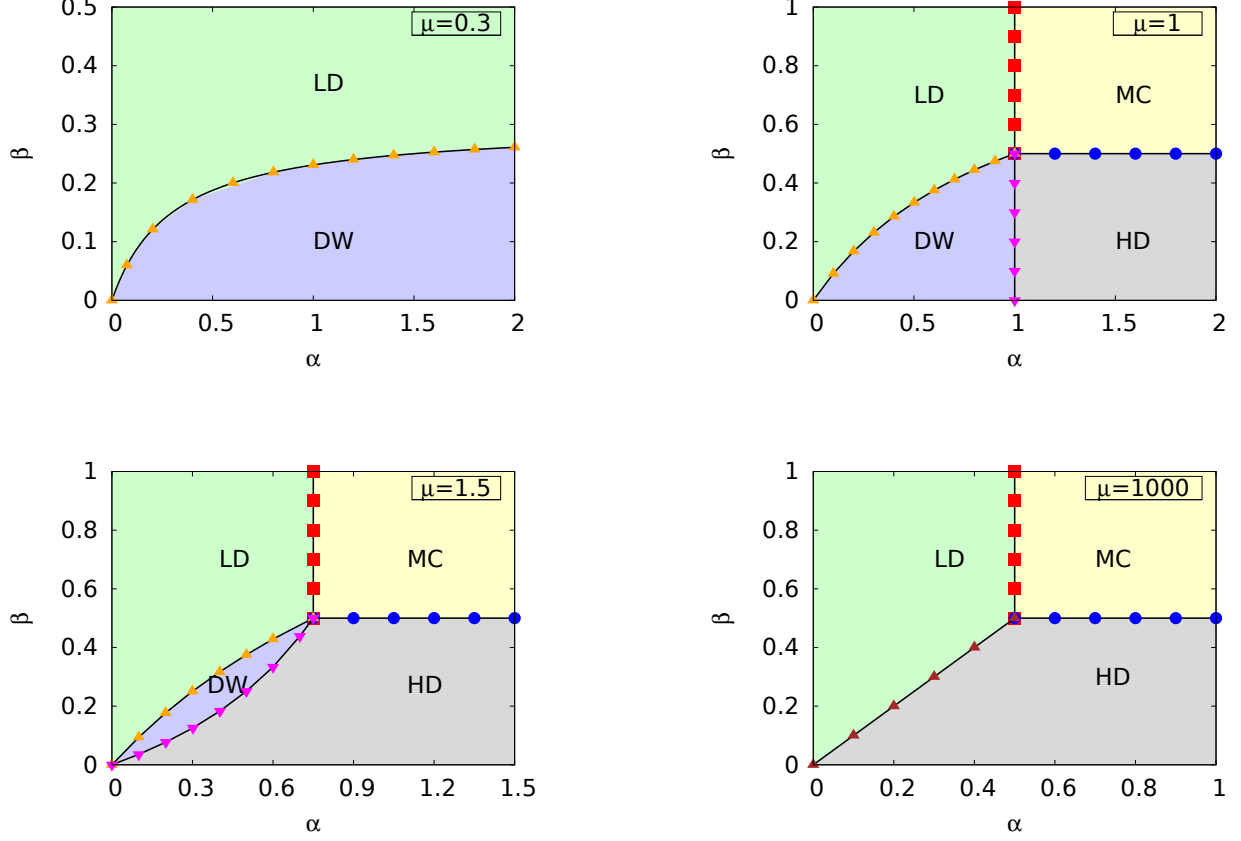


FIG. 9: Phase diagrams in the $\alpha - \beta$ plane in the strong coupling limit of the model for different values of the filling factor μ , with $k_1 = 0$ and $k_2 = 0.95$. MFT predicts up to four distinct phases (LD, HD, MC, and DW), represented by the green, gray, yellow, and blue regions, respectively, with black solid lines separating them, see Eqs. (A15), (A16), (A25), and (A26) for MFT phase boundaries. The phase boundaries obtained from MCS are depicted by colored points: red (LD-MC), blue (HD-MC), orange (LD-DW), and magenta (HD-DW). The MFT and MCS results exhibit excellent match. In the limit of large μ (say for $\mu = 1000$), the phase diagram of the present model is identical to the familiar phase diagram of an open TASEP.

strong coupling limit, we follow the logic and calculational scheme outlined above for the weak coupling limit of the model.

a. Low-density phase

We start by using Eq. (17). Last part in the right-hand side of Eq. (17) is $\mathcal{O}(1/L)$ and hence can be neglected in the thermodynamic limit ($L \rightarrow \infty$). In that limit, the quadratic equation in (17) becomes linear in ρ_{LD} , solving which we obtain

$$\rho_{LD} \approx \frac{\alpha k_2}{k_1 + \left(1 + \frac{\alpha}{\mu}\right) k_2}. \quad (\text{A2})$$

Clearly, ρ_{LD} is independent of β . Considering Eq. (A2) we find the following:

$$\rho_{LD} \xrightarrow{\mu \rightarrow 0} 0, \quad (\text{A3})$$

$$\rho_{LD} \xrightarrow{\mu \rightarrow \infty} \frac{\alpha k_2}{k_1 + k_2}. \quad (\text{A4})$$

Thus, for $\mu \rightarrow \infty$, we have $\rho_{LD} \rightarrow \alpha/2$ when $k_1 = k_2$ and $\rho_{LD} \rightarrow \alpha$ when $k_1 = 0$.

The population of reservoirs, N_1 and N_2 , can be obtained in the strong coupling limit likewise we did in the weak coupling limit, i.e., using $\rho_{LD} = \alpha N_1/N_0$ together with the PNC relation that relates N_2 with N_1 . We find:

$$N_1 = \frac{L k_2 \mu}{k_1 + \left(1 + \frac{\alpha}{\mu}\right) k_2}, \quad (\text{A5})$$

$$N_2 = \frac{L k_1 \mu}{k_1 + \left(1 + \frac{\alpha}{\mu}\right) k_2}. \quad (\text{A6})$$

As previously stated, the relative population of the reser-

voirs is determined solely by the ratio of particle exchange rates in the strong coupling limit: $N_1/N_2 = k_2/k_1$. This effectively eliminates one of the reservoirs in the strong coupling limit.

Similar to the weak coupling limit, LD phase can be present for any (positive) value of μ in the strong coupling limit. This is demonstrated in Fig. 9, where the LD phase can be found for small μ values as well as large μ values. Since $\rho_{LD} < 1/2$, one gets the following as a condition for LD phase existence according to MFT:

$$\alpha < \frac{k_1 + k_2}{\left(2 - \frac{1}{\mu}\right)k_2}. \quad (\text{A7})$$

This is illustrated in Fig. 9. For instance, when $k_1 = 0$, $k_2 = 0.95$, and $\mu = 1$ (upper right phase diagram), the condition (A7) infers an LD phase for $\alpha < 1$. Similarly when μ is very large, say $\mu = 1000$ (lower right phase diagram), LD phase is limited up to $\alpha = 0.5$ along the α -axis.

b. High-density phase

We again proceed with the reasoning presented in the weak coupling limit. Neglecting the last term of order $\mathcal{O}(1/L)$ in Eq. (26) in the thermodynamic limit, the HD phase density ρ_{HD} in the strong coupling limit can be obtained approximately as:

$$\rho_{HD} \approx \frac{k_1 + (1 - \beta)k_2}{\left(1 + \frac{\beta}{\mu}\right)k_1 + k_2}. \quad (\text{A8})$$

As expected, ρ_{HD} is independent of α . It can be shown from Eq. (A8) that

$$\rho_{HD} \xrightarrow{\mu \rightarrow \infty} \left(1 - \frac{\beta k_2}{k_1 + k_2}\right), \quad (\text{A9})$$

which for the two cases $k_1 = k_2$ and $k_1 = 0$, yields $\rho_{HD} \rightarrow (1 - \beta/2)$ and $\rho_{HD} \rightarrow (1 - \beta)$, respectively.

The reservoir populations in the HD phase can be obtained as

$$N_1 = \frac{Lk_2(\mu - 1 + \beta)}{\left(1 + \frac{\beta}{\mu}\right)k_1 + k_2}, \quad (\text{A10})$$

$$N_2 = \frac{Lk_1(\mu - 1 + \beta)}{\left(1 + \frac{\beta}{\mu}\right)k_1 + k_2}. \quad (\text{A11})$$

Again, the ratio of reservoir populations remains constant: $N_1/N_2 = k_2/k_1$.

The lower threshold of μ for HD phase existence is determined in Section A1c. Similar to the weak coupling limit case, there will be no finite upper threshold of μ for HD phase occurrence. In the phase diagrams of Fig. 9, the

occurrence of HD phase is displayed. When the value of μ is sufficiently small, such as $\mu = 0.3$, HD phase is absent due to an inadequate number of particles being available. Since $\rho_{HD} > 1/2$, we get the following condition for HD phase:

$$\beta < \frac{k_1 + k_2}{2k_2 + \frac{k_1}{\mu}}, \quad (\text{A12})$$

which implies that, for a fixed value of k_1 , k_2 , and μ HD phase exists if β satisfies the above condition. This can be readily seen in the phase diagrams Fig. 9 where we have taken $k_1 = 0$, $k_2 = 0.95$. In this case, HD phase lies under the line $\beta = 1/2$ for any value of μ .

c. Maximal current phase

With a uniform hopping rate of 1, the steady state bulk density $\rho_{MC} = 1/2$ in the MC phase. The PNC relation reads $N_0 = N_1 + N_2 + L/2$ in this phase. The maximum current J_{\max} associated with the MC phase is given by $J_{\max} = \rho(1 - \rho) = 1/4$. Analogous to the open TASEP, following are the boundary conditions in MC phase:

$$\alpha_{\text{eff}} = \alpha \frac{N_1}{N_0} > \frac{1}{2}, \quad (\text{A13})$$

$$\beta_{\text{eff}} = \beta \left(1 - \frac{N_2}{N_0}\right) > \frac{1}{2}. \quad (\text{A14})$$

The boundaries between the LD and MC phases, and between the HD and MC phases can be determined by substituting the given values of ρ_{LD} and $\rho_{HD} = 1/2$ into equations (A2) and (A8), respectively. We thus obtain following equations as the LD-MC and HD-MC boundaries respectively:

$$\alpha = \frac{\mu(k_1 + k_2)}{(2\mu - 1)k_2}, \quad (\text{A15})$$

$$\beta = \frac{\mu(k_1 + k_2)}{k_1 + 2\mu k_2}. \quad (\text{A16})$$

Considering the non-negativity of α in Eq. (A15), one finds the MC phase to exist for any $\mu > 1/2$ in the strong coupling limit. Nevertheless, β in Eq. (A16) is inherently positive. This infers no upper threshold of μ for MC phase to exist. Following is the range:

$$\frac{1}{2} < \mu < \infty. \quad (\text{A17})$$

Following the same line of argument as given in the weak coupling limit, (A17) is also the range of μ within which HD phase appears in the phase diagram, see Fig. 9.

The existence of MC phase is illustrated in Fig. 9, where it does not appear for $\mu < 1/2$ (such as $\mu = 0.3$).

d. *Domain wall phase*

In addition to the above phases with uniform density, one can also expect the emergence of a domain wall (DW) phase with non-uniform density, where the LD and HD phases are connected by a domain wall in the bulk of the TASEP lane. The precise location of this DW can be obtained by PNC, inferring it as an LDW. At this point, we determine the position x_w and height Δ of the LDW in a similar manner as done for the weak coupling limit case. By neglecting terms of order $\mathcal{O}(1/L)$ in the thermodynamic limit, we can solve the coupled equations (43) and (44) to obtain expressions for N_1/N_0 and x_w . The solutions in the strong coupling limit are as follows:

$$\frac{N_1}{N_0} = \frac{k_2}{k_1 + \frac{\alpha}{\beta}k_2}, \quad (\text{A18})$$

$$x_w = \frac{1 - \left(\frac{k_2}{k_1 + \frac{\alpha}{\beta}k_2}\right) \left[\mu \left(\frac{\alpha}{\beta} - 1\right) + \alpha \right]}{1 - 2\alpha \frac{k_2}{k_1 + \frac{\alpha}{\beta}k_2}}. \quad (\text{A19})$$

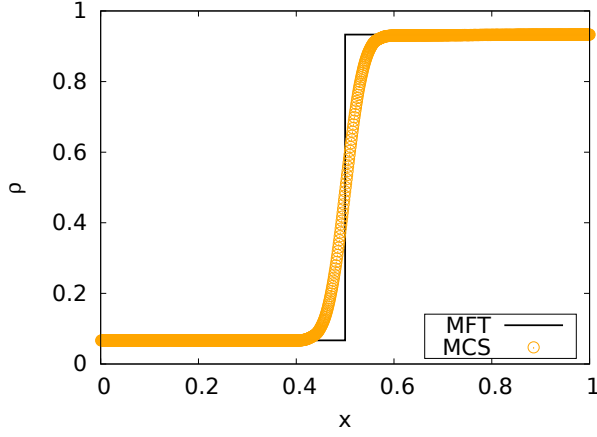


FIG. 10: Steady state density profile in the DW phase in the strong coupling limit of the model. Model parameters are: $\mu = 3/2$, $k_1 = k_2 = 0.7$, $\alpha = 0.2$ and $\beta = 0.1$. MCS results agree well with the MFT predictions given by Eqs. (A19), (A21), and (A22).

The reservoir populations, N_1 and N_2 , are related by the equation $\alpha_{\text{eff}} = \beta_{\text{eff}}$ or $\alpha N_1/N_0 = \beta(1 - N_2/N_0)$ in the DW phase, which yields the expression for N_2 :

$$\frac{N_2}{N_0} = 1 - \frac{\alpha}{\beta} \frac{N_1}{N_0} = 1 - \frac{k_2}{\frac{\beta}{\alpha}k_1 + k_2}. \quad (\text{A20})$$

The steady state low and high densities in the DW phase

are

$$\rho_{\text{LD}} = \alpha \frac{N_1}{N_0} = \frac{\alpha k_2}{k_1 + \frac{\alpha}{\beta}k_2}, \quad (\text{A21})$$

$$\rho_{\text{HD}} = 1 - \rho_{\text{LD}} = 1 - \frac{\alpha k_2}{k_1 + \frac{\alpha}{\beta}k_2}. \quad (\text{A22})$$

Then the domain wall height Δ is given by

$$\Delta = \rho_{\text{HD}} - \rho_{\text{LD}} = 1 - \frac{2\alpha\beta k_2}{\beta k_1 + \alpha k_2}. \quad (\text{A23})$$

The expression of Δ in the strong coupling limit, as given in Eq. (A23), depends only on parameters α , β , k_1 , and k_2 . Notably, it is independent of the filling factor μ .

In Fig. 11, the graph illustrates a linear decrease in the position of the domain wall (DW) as μ increases, while the height of the DW remains constant throughout the range of μ values. On the other hand, in Fig. 12, both the position and height of the DW exhibit no significant variation as k_2 changes.

Following the same arguments given in weak coupling limit of the model, the range of μ over which DW phase exists can be identified in strong coupling limit. Using the fact that DW position, x_w , should be between 0 and 1, we find this range as below:

$$\left(\frac{\alpha}{\beta} - 1\right) < \mu < \left(\frac{k_1}{k_2} + \frac{\alpha}{\beta} - \alpha\right). \quad (\text{A24})$$

Furthermore, the boundaries between the LD and DW, and between the HD and DW phases can be determined by substituting $x_w = 1$ and $x_w = 0$ respectively into Eq. (A19). The resulting equations for LD-DW and HD-DW phase boundaries are respectively:

$$\mu \left(1 - \frac{\alpha}{\beta}\right) + \alpha = 0, \quad (\text{A25})$$

$$\left(\frac{k_2}{k_1 + \frac{\alpha}{\beta}k_2}\right) \left[\mu \left(1 - \frac{\alpha}{\beta}\right) - \alpha \right] + 1 = 0. \quad (\text{A26})$$

2. Delocalization of LDW

Similar to the weak coupling limit, DWs in the strong coupling limit also gradually get delocalized with increasing μ . This is clearly shown in Fig. 13 where one can see that the domain walls get completely delocalized with $\mu \sim L$ — a fact already argued in Section VII of the main paper.

a. Phase boundaries meet at a common point

For specific values of μ when all four phases (LD, HD, MC, and DW) exist, they intersect in the $\alpha - \beta$ plane at a

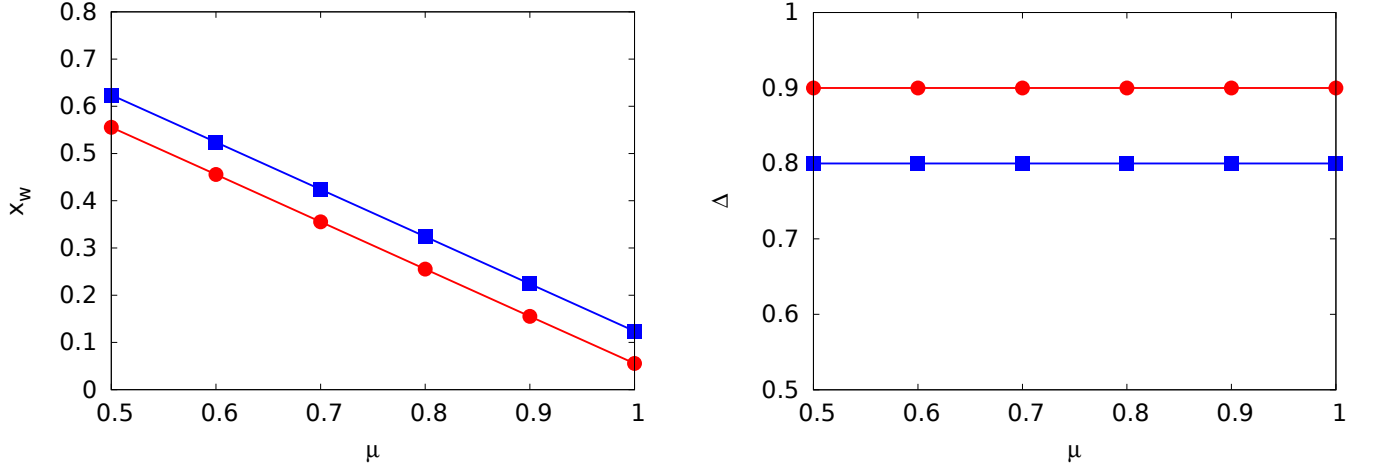


FIG. 11: **(Left)** Plots of DW position (x_w) vs. the filling factor (μ) in the strong coupling limit of the model. The exchange rates are set to $k_1 = 0$ and $k_2 = 0.95$, while two different sets of entry and exit rate parameters are considered: $\alpha = 0.5$ with $\beta = 0.05$ (red) and $\alpha = 0.5$ with $\beta = 0.1$ (blue). Solid lines represent the predictions from MFT [see Eq. (A19)], while the discrete points correspond to the results obtained through MCS. Within the given range of μ , the x_w linearly decreases with increasing μ . **(Right)** Plots of DW height (Δ) as a function of the filling factor (μ) in the strong coupling limit of the model. The parameter values for this plot are the same as those used in the left plot, with matching colors. Notably, Δ remains unchanged as μ varies within the examined range, see Eq. (A23). Both MFT and MCS results are in good agreement.

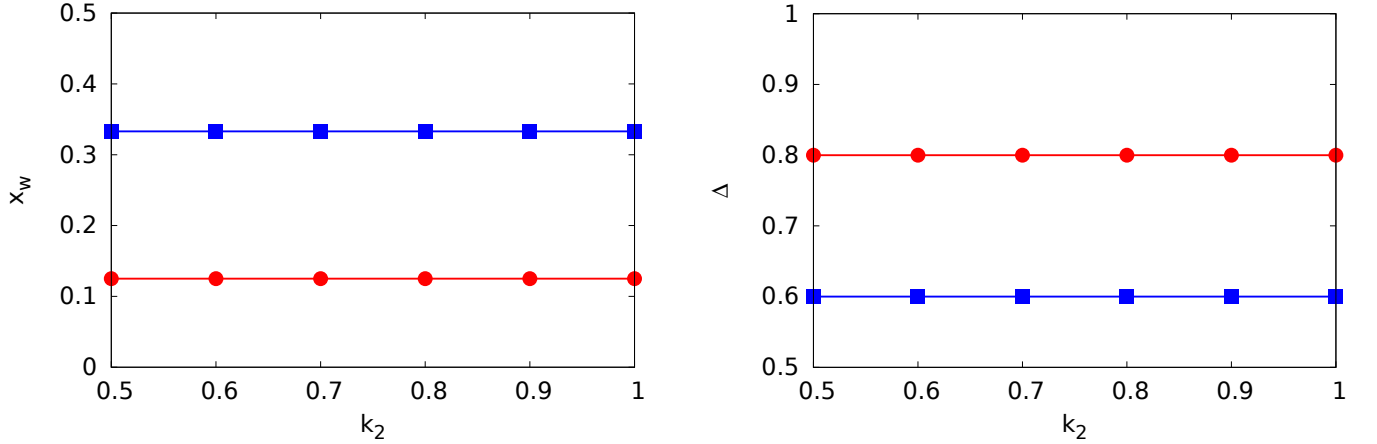


FIG. 12: **(Left)** Plots of DW position (x_w) vs. k_2 in the strong coupling limit of the model when $k_1 = 0$. The red plot corresponds to $\alpha = 0.5$ and $\beta = 0.1$, while the blue plot represents $\alpha = 0.5$ and $\beta = 0.2$. The position of DW does not vary with k_2 , see Eq. (A19). **(Right)** Plots of DW height (Δ) vs. k_2 in the strong coupling limit with $k_1 = 0$. The red and blue plots correspond to the same parameter values as in the left graph. MCS outcomes satisfy MFT predictions, see Eq. (A23).

common single point. This point, which is named (four-phase) multicritical point, can be obtained as the meeting point of all four phase boundaries in Eqs. (A15), (A16), (A25), and (A26):

$$(\alpha_c, \beta_c) = \left(\frac{\mu(k_1 + k_2)}{(2\mu - 1)k_2}, \frac{\mu(k_1 + k_2)}{k_1 + 2\mu k_2} \right). \quad (\text{A27})$$

Depending explicitly on k_1 , k_2 , and μ this unique point exists for any value of μ greater than $1/2$, above which all four phases appear in the phase diagram, see Fig. 9. The distance between the origin $(0,0)$ and the multicritical

point (α_c, β_c) can be calculated using the formula:

$$d = \sqrt{\left(\frac{\mu(k_1 + k_2)}{(2\mu - 1)k_2} \right)^2 + \left(\frac{\mu(k_1 + k_2)}{k_1 + 2\mu k_2} \right)^2}. \quad (\text{A28})$$

Appendix B: Simulation algorithm

In this study, the mean-field predicted densities and phase diagrams of the model were validated through Monte Carlo simulations using random updates. The

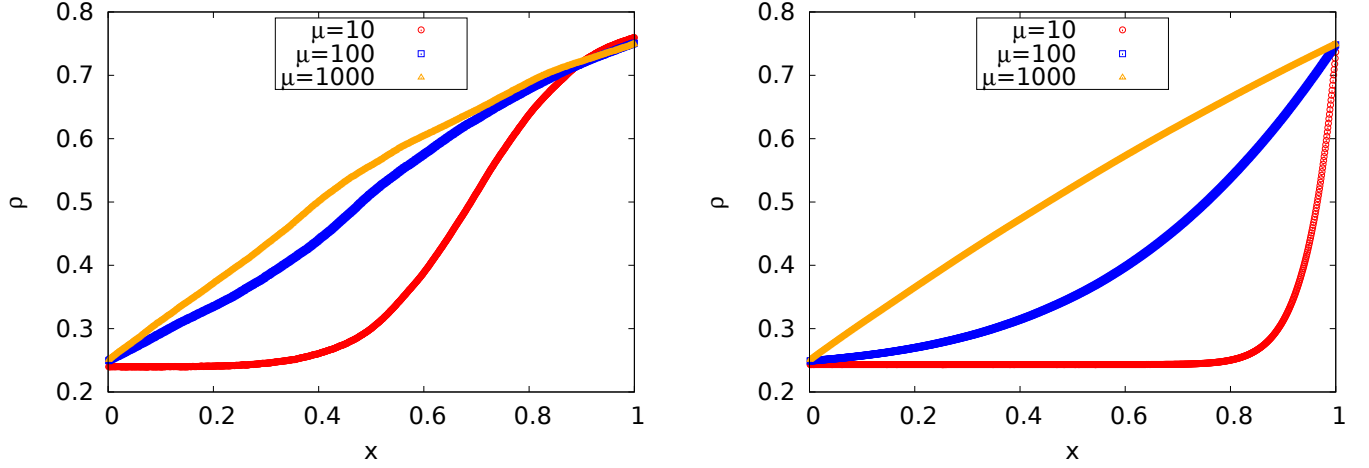


FIG. 13: Gradual delocalization of DW with increase in μ . **(Left)** This corresponds to the weak coupling limit. Parameter values are: $\alpha = 0.25$, $\beta = 0.24$, $\mu = 10$, $k_{10} = 0$, and $k_{20} = 0.95$ (red circles); $\alpha = 0.25$, $\beta = 0.2488$, $\mu = 100$, $k_{10} = 0$, and $k_{20} = 0.95$ (blue squares); and $\alpha = 0.25$, $\beta = 0.24985$, $\mu = 1000$, $k_{10} = 0$, and $k_{20} = 0.95$ (orange triangles). **(Right)** This corresponds to the strong coupling limit. Parameter values are: $\alpha = 0.25$, $\beta = 0.24985$, $\mu = 10$, $k_{10} = 0$, and $k_{20} = 0.95$ (red circles); $\alpha = 0.25$, $\beta = 0.24985$, $\mu = 100$, $k_{10} = 0$, and $k_{20} = 0.95$ (blue squares); and $\alpha = 0.25$, $\beta = 0.24985$, $\mu = 1000$, $k_{10} = 0$, and $k_{20} = 0.95$ (orange triangles). For both weak and strong coupling limits, system size $L = 1000$ and averages over 2×10^9 times steps are done to get the MCS density profiles. Clearly, the LDW for smaller values of μ gets delocalized as $\mu \sim L$.

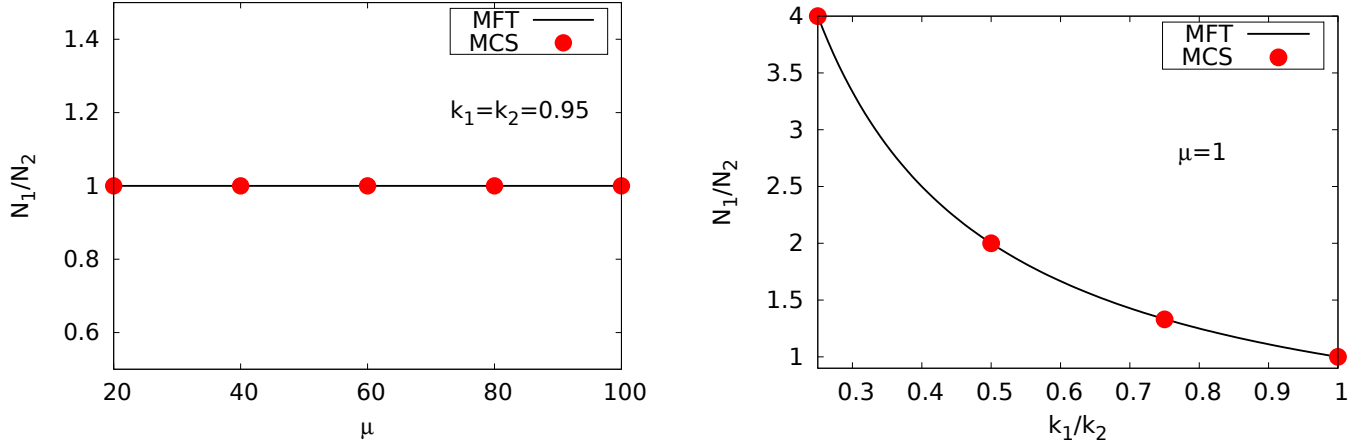


FIG. 14: **(Left)** Plot showing dependence of the reservoir population ratio N_1/N_2 on μ in the strong coupling limit of the model. **(Right)** Plot presenting the variation of the reservoir population ratio N_1/N_2 with k_1/k_2 for a fixed filling factor $\mu = 1$ in the strong coupling limit. In these plots, the entry and exit rates are carefully selected to ensure that the TASEP lane remains in the LD phase. The values of $\alpha = 0.1$ and $\beta = 1$ are used. The results obtained by MFT and MCS are in good agreement.

simulation rules are as follows: (i) If the first site ($i = 1$) of the TASEP lane (T) is empty, a particle from reservoir R_1 enters T with a rate α_{eff} ; (ii) Particles in T can hop with rate 1 to the next site in the bulk of T provided that site is empty; (iii) Upon reaching the last site ($i = L$) of T , a particle exits with a rate β_{eff} into reservoir R_2 ; (iv) Concurrently, particles in the reservoirs (R_1

and R_2) can jump directly to the other reservoir with rates k_1 from R_1 to R_2 and k_2 from R_2 to R_1 . The above dynamical update rules were implemented with random sequential updates. After sufficient number of iterations (typically 10% to 30% of the total number of time steps) were performed to reach a steady state, time-averaged density profiles were obtained.

[1] C. T. MacDonald, J. H. Gibbs, and A. C. Pipkin, “Kinetics of biopolymerization on nucleic acid templates”,

Biopolymers **6**, 1 (1968).

- [2] J. Krug, “Boundary-induced phase transitions in driven diffusive systems”, *Phys. Rev. Lett.* **67**, 1882 (1991).
- [3] B. Derrida, S. A. Janowsky, J. L. Lebowitz, and E. R. Speer, “Exact solution of the totally asymmetric simple exclusion process: Shock profiles”, *J Stat Phys*, 813–842.
- [4] B. Derrida and M. R. Evans, “Exact correlation functions in an asymmetric exclusion model with open boundaries”, *Journal de Physique I* **3**, 311–322 (1993).
- [5] T. Chou, K. Mallick, and R. K. P. Zia, “Non-equilibrium statistical mechanics: from a paradigmatic model to biological transport”, *Rep. Prog. Phys.* **74**, 116601 (2011).
- [6] S. A. Janowsky and J. L. Lebowitz, “Finite-size effects and shock fluctuations in the asymmetric simple-exclusion process”, *Phys. Rev. A* **45**, 618 (1992).
- [7] N. Sarkar and A. Basu, “Nonequilibrium steady states in asymmetric exclusion processes on a ring with bottlenecks”, *Phys. Rev. E* **90**, 022109 (2014).
- [8] G. Tripathy and M. Barma, “Driven lattice gases with quenched disorder: Exact results and different macroscopic regimes”, *Phys. Rev. E* **58**, 1911 (1998).
- [9] H. Hinsch and E. Frey, “Bulk-driven nonequilibrium phase transitions in a mesoscopic ring”, *Phys. Rev. Lett.* **97**, 095701 (2006).
- [10] T. Banerjee, N. Sarkar, and A. Basu, “Generic nonequilibrium steady states in an exclusion process on an inhomogeneous ring”, *J. Stat. Mech. J. Stat. Mech.* P01024 (2015).
- [11] P. Roy, A. K. Chandra, and A. Basu, “Pinned or moving: States of a single shock in a ring”, *Phys. Rev. E* **102**, 012105 (2020).
- [12] T. Banerjee and A. Basu, “Smooth or shock: Universality in closed inhomogeneous driven single file motions”, *Phys. Rev. Research* **2**, 013025 (2020).
- [13] A. Goswami, R. Chatterjee, and S. Mukherjee, “Defect versus defect: Stationary states of single file marching in periodic landscapes with road blocks”, *arXiv: 2402.08499* (2024).
- [14] D. A. Adams, B. Schmittmann, and R. K. P. Zia, “Far from equilibrium transport with constrained resources”, *J. Stat. Mech.: Theory Exp* **2008**, P06009 (2008).
- [15] L. Jonathan Cook and R. K. P. Zia, “Feedback and fluctuations in a totally asymmetric simple exclusion process with finite resources”, *J. Stat. Mech.: Theory Exp* **2009**, P02012 (2009).
- [16] L. Jonathan Cook, R. K. P. Zia, and B. Schmittmann, “Competition between multiple totally asymmetric simple exclusion processes for a finite pool of resources”, *Phys. Rev. E* **80**, 031142 (2009).
- [17] M. Ha and M. den Nijs, “Macroscopic car condensation in a parking garage”, *Phys. Rev. E* **66**, 036118 (2002).
- [18] C. A. Brackley, M. C. Romano, C. Grebogi, and M. Thiel, “Limited resources in a driven diffusion process”, *Phys. Rev. Lett.* **105**, 078102 (2010).
- [19] C. A. Brackley, M. C. Romano, and M. Thiel, “Slow sites in an exclusion process with limited resources”, *Phys. Rev. E* **82**, 051920 (2010).
- [20] C. A. Brackley, M. C. Romano, and M. Thiel, “The dynamics of supply and demand in mRNA translation”, *PLoS computational biology* **7**, e1002203 (2011).
- [21] L. Ciandrini, I. Neri, J. C. Walter, O. Dauloudet, and A. Parmeggiani, “Motor protein traffic regulation by supply-demand balance of resources”, *Phys. Biol.* **11**.
- [22] M. C. Good, M. D. Vahey, A. Skandarajah, D. A. Fletcher, and R. Heald, “Cytoplasmic volume modulates spindle size during embryogenesis”, *Science* **342**, 856–860 (2013).
- [23] J. Hazel, K. Krutkramelis, P. Mooney, M. Tomschik, K. Gerow, J. Oakey, and J. C. Gatlin, “Changes in cytoplasmic volume are sufficient to drive spindle scaling”, *Science* **342**, 853 (2013).
- [24] A. Robson, K. Burrage, and M. C. Leake, “Inferring diffusion in single live cells at the single-molecule level”, *Philos Trans R Soc (Lond) B Biol Sci.* **368**(1611), 20120029 (2013) [doi: 10.1098/rstb.2012.0029].
- [25] R. Lipowsky, S. Klumpp, and T. M. Nieuwenhuizen, “Random walks of cytoskeletal motors in open and closed compartments”, *Phys. Rev. Lett.* **87**, 108101 (2001).
- [26] S. Klumpp and R. Lipowsky, “Traffic of molecular motors through tube-like compartments”, *Journal of Statistical Physics* **113**, 233 (2003).
- [27] S. Klumpp and R. Lipowsky, “Asymmetric simple exclusion processes with diffusive bottlenecks”, **70**, 066104 (2004).
- [28] L. D. Fernandes and L. Ciandrini, “Driven transport on a flexible polymer”, *Phys. Rev. E* **99**, 052409 (2019).
- [29] O. Dauloudet *et al.*, “Modelling the effect of ribosome mobility on the rate of protein synthesis”, *Eur. Phys. J. E* **44**, 19 (2021).
- [30] I. R. Graf and E. Frey, “Generic Transport Mechanisms for Molecular Traffic in Cellular Protrusions”, *Phys. Rev. Lett.* **118**, 128101 (2017).
- [31] M. Bojer, I. R. Graf, and E. Frey, “Self-organized system-size oscillation of a stochastic lattice-gas model”, *Phys. Rev. E* **98**, 012410 (2018).
- [32] A. Goswami, M. Chatterjee, and S. Mukherjee, “Steady states and phase transitions in heterogeneous asymmetric exclusion processes”, *J. Stat. Mech. - Th. Exp.* **123209** (2022).
- [33] S. Pal, P. Roy and, A. Basu, “Availability, storage capacity, and diffusion: Stationary states of an asymmetric exclusion process connected to two reservoirs”, *arXiv: 2308.08384*.
- [34] A. Haldar, P. Roy, and A. Basu, “Asymmetric exclusion processes with fixed resources: Reservoir crowding and steady states”, *Phys. Rev. E* **104**, 034106 (2021).
- [35] B. Pal and A. K. Gupta, “Reservoir crowding in a resource-constrained exclusion process with a dynamic defect”, *Phys. Rev. E* **106**, 044130 (2022).
- [36] N. Bhatia and A. K. Gupta, “Role of site-wise dynamic defects in a resource-constrained exclusion process”, *Chaos, Solitons and Fractals* **167**, 113109 (2023).
- [37] A. Gupta, B. Pal, and A. K. Gupta, “Interplay of reservoirs in a bidirectional system”, *Phys. Rev. E* **107**, 034103 (2023).
- [38] R. A. Blythe and M. R. Evans, “Nonequilibrium steady states of matrix-product form: a solver’s guide”, *J. Phys. A* **40**, R333 (2007).
- [39] T. Reichenbach, T. Franosch, and E. Frey, “Domain wall delocalization, dynamics and fluctuations in an exclusion process with two internal states”, *Eur. Phys. J. E* **27**, 47 (2008).